Deep-Sea Research II 122 (2015) 195–225

Contents lists available at ScienceDirect

Deep-Sea Research II

journal homepage: www.elsevier.com/locate/dsr2

Depleted deep South China Sea $\delta^{13}C$ paleoceanographic events in response to tectonic evolution in Taiwan–Luzon Strait since Middle Miocene

Wen-Huang Chen [a,b], Chi-Yue Huang [a,c,*], Yen-Jun Lin [c], Quanhong Zhao [d], Yi Yan [a,**], Duofu Chen [a], Xinchang Zhang [a,b], Qing Lan [a,b], Mengming Yu [a,b]

[a] Key Laboratory of Marginal Sea Geology, Guangzhou Institute of Geochemistry, Chinese Academy of Sciences, Guangzhou 510640, China
[b] University of Chinese Academy of Sciences, Beijing 100049, China
[c] Department of Earth Sciences, National Cheng Kung University, Tainan 701, Taiwan
[d] State Key Laboratory of Marine Geology, Tongji University, Shanghai 200092, China

ARTICLE INFO

Available online 7 February 2015

Keywords:
South China Sea paleoceanography
Taiwan Island–Luzon Strait
Subduction–collision tectonics
Closure of interarc water gate
Deep water

ABSTRACT

The most distinctive feature of the deep South China Sea (SCS) paleoceanography is the occurrence of long-term depleted deep-sea benthic foraminiferal $\delta^{13}C$ values. They are lower than the global and the Pacific composite records in the last 16 Ma, especially at 13.2, 10.5, 6.5, 3.0 and 1.2–0.4 Ma. This distinct deep SCS paleoceanograhic history coincides with the subduction–collision history in the Taiwan region where waters of the West Pacific (WP) and the SCS exchange. The depleted deep-sea benthic foraminiferal $\delta^{13}C$ events indicate that the SCS deep basin became progressively a stagnant environment in the last 16 Ma due to either closure of the connection with the WP bottom water or temporary reduction of the WP deep water flowing into the deep SCS. Both the Taiwan accretionary prism and the Luzon arc became the main tectono-morphological barriers for the WP bottom water flowing into the SCS deep basin when eastward subduction of the SCS oceanic lithosphere beneath the Philippine Sea Plate started from the Middle Miocene (18–16 Ma). This began a long-term trend of depleted SCS deep-sea benthic $\delta^{13}C$ values in the last 16 Ma. The oblique arc–continent collision since ~6.5 Ma uplifted the Taiwan accretionary prism rapidly above sea level and further isolated the SCS from the open Pacific. The collision simultaneously causes backthrusting deformations in the North Luzon Trough forearc basin and sequentially closes interarc water gates between volcanic islands from north to south. The Loho and the Taitung interarc water gates in the advanced collision zone were closed at ~3.0 Ma and ~1.2 Ma, coinciding with the very low SCS deep-sea benthic $\delta^{13}C$ events at 3.0 and 1.2–0.4 Ma, respectively. The Taitung Canyon between the Lutao and Lanyu volcanic islands in the incipient collision zone is semi-closed presently. These closure events also lead to the result that the WP deep water intrudes westward into the SCS principally through the Bashi Channel between the Lanyu and Batan volcanic islands in the subduction zone.

1. Introduction

Opening or closing of oceanic gateways controls global ocean circulations and leads to significant paleoceanographic changes (Kennett, 1982; Crowley and Burke, 1998). For example, openings of the Tasman Sea between the Australian and Antarctic continents and the Drake Passage between the South American and Antarctic continents in the early Cenozoic resulted in formation of the Antarctic Circumpolar Current (e.g. Kennett et al., 1972; Lagabrielle et al., 2009). Closures of the Indonesian Seaway between the Pacific and Indian Oceans in the Middle–Late Miocene and the Panama Seaway between the Atlantic and Pacific Oceans in the Pliocene changed the global ocean surface circulations (e.g. Haug and Tiedemann, 1998; Linthout et al., 1997). The South China Sea (SCS) is the largest marginal sea (Fig. 1A; 3.5×10^6 km^2 in area and 4700 m deep in average in the deep basin) between the Asian Continent and the Pacific Ocean. It is separated from the West Pacific (WP) by two tectono-morphological barriers of the Hengchun Ridge accretionary prism and the Luzon volcanic arc in the Luzon Strait between the Taiwan and Luzon Islands (Fig. 1A and B). Presently, the WP and SCS

* Corresponding author at: Key Laboratory of Marginal Sea Geology, Guangzhou Institute of Geochemistry, Chinese Academy of Sciences, Guangzhou 510640, China
** Correspondence to: No. 511 Kehua Street, Tianhe District, Guangzhou 510640, China. Tel.: +86 20 85290293.
E-mail addresses: huangcy@mail.ncku.edu.tw (C.-Y. Huang), yanyi@gig.ac.cn (Y. Yan).

http://dx.doi.org/10.1016/j.dsr2.2015.02.005
0967-0645/

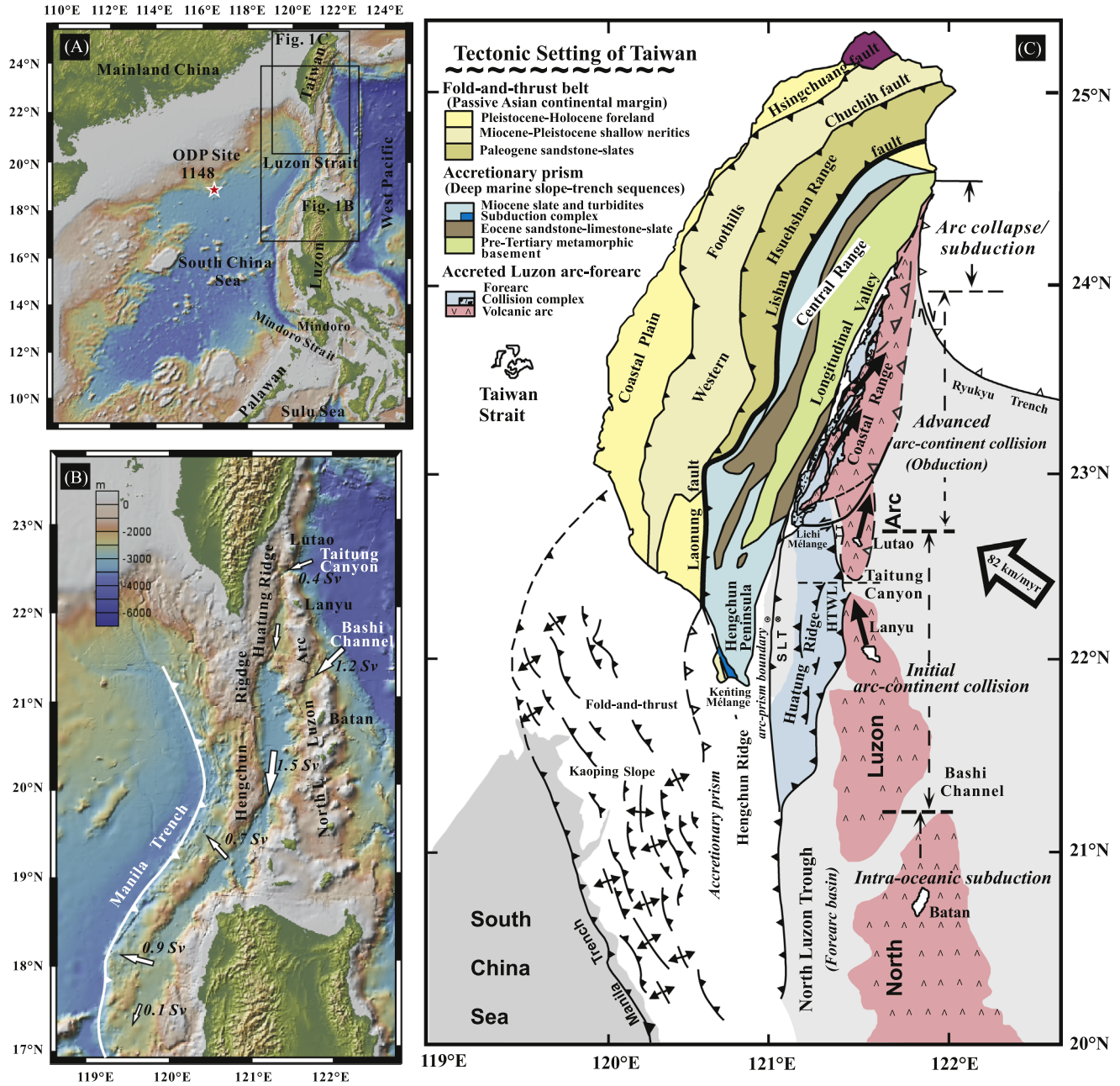

Fig. 1. Topographic map of (A) the South China Sea and (B) the region between Taiwan and Luzon Islands (adapted from Ryan et al., 2009). The red star in A marks the location of ODP Site 1148. The white arrows in B denote the route of WP deep water overflowing into the SCS. Fluxes are in Sverdrups ($1\ Sv = 1 \times 10^6\ m^3\ s^{-1}$) beside respective arrow (Zhao et al., 2014). (C) Tectonic setting of Taiwan (modified from Huang et al., 2006). Four geodynamic processes are now operating offshore and onland Taiwan from south to north: intra-oceanic subduction, initial arc–continent collision, advanced arc–continent collision and arc collapse/subduction. Open arrow shows the vector of the Philippine Sea Plate movement relative to the Eurasian Continent (Yu et al., 1997). Solid arrows show the paleomagnetic declination and diachronic clockwise rotation of four volcanic islands of the Luzon arc (from north to south: Chimei: 4–3 Ma; Chengkuangao: 2–1 Ma; Lutao: Recently; Lanyu: not rotate yet; Yang et al., 1983; Lee et al., 1991). SLT=Southern Longitudinal Trough; TT=Taitung Trough remnant forearc basin; HTWL=late deformed Huatung Ridge west of the Lanyu volcanic island. (For interpretation of the references to color in this figure legend, the reader is referred to the web version of this article.)

waters exchange through the Luzon Strait like a sandwich: the WP surface water above 300 m depth intrudes westward into the SCS (especially during the Asian summer monsoon season), water in the intermediate layer (350–1350 m depth) extrudes eastward from the SCS to the WP, and the WP deep water below 1500 m intrudes westward into the deep SCS (Wyrtki, 1961; Chen and Huang, 1996; Qu et al., 2006; Tian et al., 2006; Zhao et al., 2014). Tectono-morphological barriers of the Hengchun Ridge and the Luzon arc thus behave as thresholds controlling the SCS paleoceanography, and especially its deep-water history since these tectono-morphological barriers formed in the Middle Miocene (Huang et al., 1997, 2000).

Presently, the WP deep water flows westward into the SCS through two interarc water gates of the Luzon arc between the volcanic islands off SE Taiwan (Fig. 1B; Zhao et al., 2014): 0.4 Sv ($1\ Sv = 1 \times 10^6\ m^3\ s^{-1}$) through the Taitung Canyon (~3000 m water depth) between the Lutao and Lanyu volcanic islands in the north; 1.2 Sv through the Bashi Channel (~2400 m water depth) between the Lanyu and Batan volcanic islands in the south. The westward-intruding WP deep water then detours southward along the axis of the N–S-trending North Luzon Trough forearc basin (1.5 Sv; basin floor: ~3500 m water depth) between the Hengchun Ridge accretionary prism in the west and the Luzon volcanic arc in the east. The WP deep water then enters westward

through the Hengchun Ridge south of 20°N into the SCS deep basin (Fig. 1B; Tian and Qu, 2012; Zhao et al., 2014). The Hengchun Ridge and the Luzon arc prevent the WP bottom water (below 2500 m depth) from connecting with the SCS deep water. Therefore, along 20°N transect in 2500–3500 m depth, the dissolved oxygen concentration of the WP bottom water is much higher (2.9–3.4 mL/L) than it is in the SCS deep basin (2.5–2.7 mL/L; Qu et al., 2006).

ODP Site 1148 (18°50′N, 116°34′E, northern slope of the SCS; water depth: 3294 m; Fig. 1A) provides a continuous, high-resolution, Miocene paleoceanographic record of this tropical-subtropical marginal sea (Wang et al., 2003; Tian et al., 2008). Previous studies (Wang et al., 2003; Wang, 2012; Jian et al., 2003; Li et al., 2006, 2007; Zhao et al., 2009) showed that the most distinctive feature of the deep SCS paleoceanography is a long term trend of much depleted deep-sea benthic foraminiferal $\delta^{13}C$ values lower than the global composite record of Zachos et al. (2001) in the last 16 Ma (Fig. 2). They are especially low at 13.2, 10.5, 6.5, 3.0 and 1.2–0.4 Ma.

Previous study on the deep SCS benthic $\delta^{13}C$ paleoceanography mainly focused on the significance of the negative excursion in the last 1.4 Ma. The depleted benthic $\delta^{13}C$ in the deep SCS may be attributed to a reduction of deep-water ventilation due to an isolation of the SCS deep basin from the Pacific during glaciations (Jian et al., 2003) or to changes of regional physical-chemical conditions in the SCS deep basin due to intensive tectonics of subduction–collision in the Taiwan region since the Middle Miocene (Wang et al., 2003; Wang, 2012; Li et al., 2007; Zhao et al., 2009; Huang et al., 2012). However, neither the mechanism nor the timing of the tectonic events related to the depleted benthic $\delta^{13}C$ in the deep SCS has been specifically discussed as yet.

It is quite peculiar that more WP deep water passes through the shallow Bashi Channel (~2400 m) in the south than through the deep Taitung Canyon (~3000 m) in the north (Fig. 1B). Could tectonics in the Luzon arc or/and the North Luzon Trough forearc basin off SE Taiwan play an important role in control of such a variation of the WP deep water flux through these interarc water gates? If this proposed mechanism is convincible, did tectonics occurring in ancient interarc water gates north of present Taitung Canyon also play a similar role in control of the westward intrusion of the WP deep water? When did these ancient interarc water gates close in response to tectonics? Did these closure events coincide with the very low $\delta^{13}C$ value events of deep SCS paleoceanographic record in the last 16 Ma?

Thus, this study addresses the geological relationship between the deep SCS paleoceanography, especially the depleted deep-sea benthic foraminiferal $\delta^{13}C$ events at 13.2, 10.5, 6.5, 3.0 and 1.2–0.4 Ma, and tectonic developments in the Taiwan Island–Luzon Strait region where the WP deep water intrudes westwards into the deep SCS. Particularly, a new biostratigraphic study on the Coastal Range is conducted to illuminate the closure events of ancient interarc water gates between volcanic islands.

2. Regional geology of the Luzon Strait and Taiwan Island

The Luzon Strait and Taiwan Island are located at the convergent plate boundary between the Eurasian Continent in the west and the Philippine Sea Plate in the east (Fig. 1A). The SCS oceanic lithosphere rifted from the Eurasian Continent in the Oligocene–Middle Miocene (Taylor and Hayes, 1983) and subducts eastward beneath the Philippine Sea Plate along the Manila trench (Fig. 1B; Tsai, 1986). Subduction develops the Hengchun Ridge accretionary prism, North Luzon Trough forearc basin and Luzon arc in the Luzon Strait between the Taiwan and Luzon Islands (Fig. 1B; Huang et al., 1992, 1997). The Luzon arc on the Philippine Sea Plate is moving northwestward towards the Asian continental

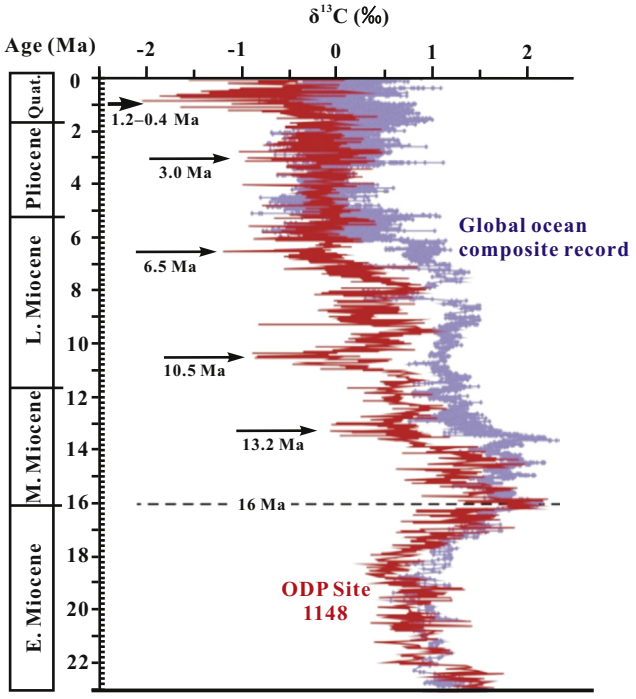

Fig. 2. Downhole variations of benthic foraminiferal $\delta^{13}C$ at ODP Site 1148 (Tian et al., 2008), as compared to the global composite record (Zachos et al., 2001) (adapted from Wang, 2012). The arrows denote the unusual low value events of benthic $\delta^{13}C$ at ODP Site 1148.

margin (060°) and has been colliding with the Eurasian Plate obliquely in the last 6.5 Ma (Huang et al., 2000, 2006). The oblique collision propagates southward in a speed of 84 km/my (Suppe, 1984). These marine geological units and structures in the Luzon Strait extend northward to be exposed on Taiwan (Fig. 1B and C).

The Taiwan Island is composed of three major geological units, from west to east, the Coastal Plain–Western Foothills–Hsüehshan Range of the fold-and-thrust belt, the Central Range–Hengchun Peninsula of the accretionary prism, and the Coastal Range of the volcanic arc and forearc basin (Fig. 1C; Huang et al., 2000, 2006). The Coastal Plain–Western Foothills–Hsüehshan Range on Taiwan are equivalent to the newly developed Kaoping Slope west of the Hengchun Ridge off SE Taiwan (Fig. 1C). They represent the most recent deformed passive margin sequences during the arc–continent collision. The Hengchun Ridge accretionary prism extends northward to the onshore Hengchun Peninsula–Central Range, while the North Luzon Trough forearc basin and the Luzon volcanic arc connect northward to the Coastal Range in eastern Taiwan (Fig. 1C). However, except the Luzon volcanic arc, neither the Hengchun Ridge accretionary prism nor the North Luzon Trough forearc basin is exposed on Luzon Island (Fig. 1B). South of 20°N, the accretionary prism and forearc basin extend southwestward to the offshore area west of Luzon and disappear between Luzon and Mindoro as the Palawan–Mindoro continental block collides with the Philippine Mobile Belt (Fig. 1A; Yumul et al., 2009). Thus, the geological units onland Taiwan and their offshore equivalents in the Luzon Strait provide unique materials for understanding the tectonic evolution of the water gateway between the SCS and the WP.

Four tectonic processes are operating today between Luzon and Taiwan. From south to north, they are: intra-oceanic subduction, initial arc–continent collision, advanced arc–continent collision (or obduction), and arc collapse/subduction (Fig. 1C; Huang et al., 2000). Because of the southward propagation of arc–continent collision, the spatial pattern of these tectonic processes is equivalent to temporal orogenic processes on Taiwan since the Middle Miocene (Suppe, 1981; Huang et al., 2000, 2006). In this discussion

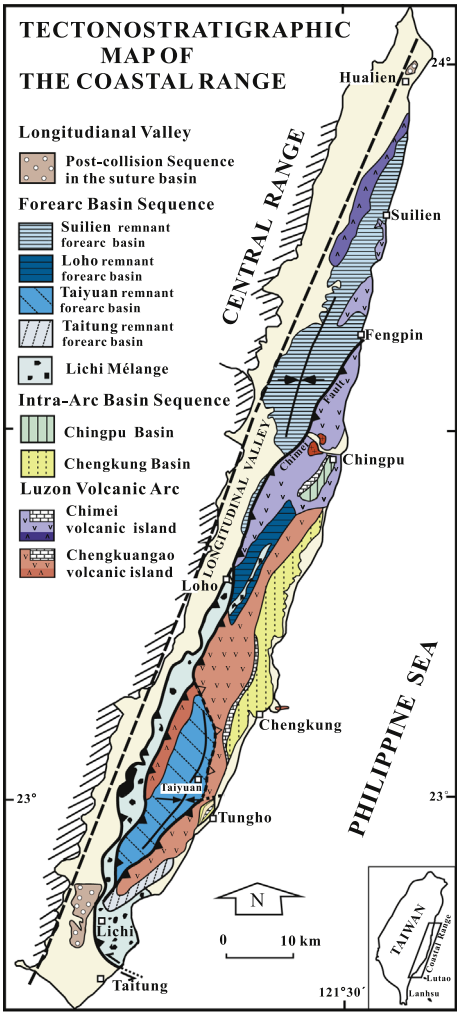

Fig. 3. Tectonostratigraphic map of the Coastal Range (revised from Huang et al., 1995, 2006). The Coastal Range consists of four remnant forearc basins, two volcanic islands associated with two intra-arc basins and a forearc collisional mélange. The volcanic islands are composed of andesites, agglomerates and tuffs of the Tuluanshan Formation, whereas the remnant forearc basins and the intra-arc basins are composed of stratified deep-sea turbidites of the Takangkou and the Chimei Formations mostly derived from the accretionary prism (Hsu, 1956).

the Central Range–Hengchun Peninsula and marine Hengchun Ridge are combined together as the Taiwan accretionary prism.

The Coastal Range in the advanced arc–continent collision zone is composed of two independent volcanic islands (Chimei volcanic island in the north and Chengkuangao volcanic island in the south) with two intra-arc basins, four remnant forearc basins (from north to south: Suilien, Loho, Taiyuan and Taitung) and a forearc collisional Lichi Mélange (Fig. 3; Huang et al., 1995, 2006, 2008). Four remnant forearc basins were parts of a continuous North Luzon Trough forearc basin. They were separated by thrusting during the incipient arc–continent collision. The Suilien and the Taiyuan remnant forearc basins are much larger than the Loho and the Taitung remnant forearc basins (Fig. 3). Previous paleogeographic reconstructions (Huang et al., 1995, 2006) showed that the Suilien remnant forearc basin was located west of the Chimei volcanic island and the Taiyuan remnant forearc basin was situated west of the Chengkuangao volcanic island (Fig. 3). In contrast, the Loho remnant forearc basin was located near the interarc passage between the Chimei and Chengkuangao volcanic islands, while the Taitung remnant forearc basin was situated near the interarc passage between the onland Chengkuangao volcanic island and the offshore Lutao volcanic island (Fig. 3).

Paleogeography of the Loho and the Taitung remnant forearc basins is analogous to the modern "HTWL" (late deformed Huatung Ridge west of the Lanyu volcanic island; Figs. 1C and 11) which connects to the interarc passage of the Taitung Canyon between the Lutao and Lanyu volcanic islands in the incipient collision zone (see Section 5.4). The geological role of the HTWL in the incipient collision zone has been studied by Huang et al. (unpublished results). In the present paper, the interarc passage between the Chimei and Chengkuangao volcanic islands is named the Loho interarc water gate. Likewise, the interarc passage between the Chengkuangao and Lutao volcanic islands is named the Taitung interarc water gate (Fig. 11). Therefore, the youngest depositional age of the two remnant forearc basins indicates the time when these interarc water gates were closed.

3. Study methods

Three tectonic events might have controlled water exchanges between the deep SCS and the WP: (1) initiation event of the SCS subduction beneath the Philippine Sea Plate to develop two tectono-morphological barriers of the Taiwan accretionary prism and the Luzon arc, (2) sub-aerial exposure event of the Taiwan accretionary prism to narrow the water gateway between the SCS and the WP, and (3) closure events of the interarc water gates between volcanic islands, through which the WP deep water intrudes into the SCS. For the first and second, we review published surveys in the modern subduction–collision zones off southern Taiwan and stratigraphy on Taiwan. Correlations and age determinations for the third are documented here.

Closures of the Loho and the Taitung interarc water gates are dated by detailed study on integrated biostratigraphy of both planktonic foraminifera and calcareous nannofossils in the Loho and the Taitung remnant forearc basins (Figs. 4A and 6). These new study results are shown in Figs. 5 and 7 and listed in Appendices A and B, respectively.

Planktonic foraminifera are separated from 200 grams of mudstone by conventional methods. Foraminiferal tests off the 100-mesh screen are picked for identifications under stereomicroscope or/and scanning electron microscope (SEM; Fig. 8). Standard zonations of planktonic foraminifera established from low-latitude regions by Blow (1969) and datum planes (FAD: First appearance datum; LAD: last appearance datum) documented by Wade et al. (2011) are followed. Five to ten grams of each sample is selected for calcareous nannofossils study using standard smear-slide techniques (Bown and Young, 1998). For each slide, more than 100 fields of view (FOV) are examined randomly under a polarizing microscope with 1600 fold magnification (Fig. 9). Five classes are used to denote floral abundances (abundant: >100 specimens/20 FOV; common: 51–100 specimens/20 FOV; few: 21–50 specimens/20 FOV; rare: 2–20 specimens/20 FOV; present: only 1 specimen/≥ 20 FVO). Zonal scheme of calcareous nannofossils proposed by Martini (1971) and datum planes compiled by Anthonissen and Ogg (2012) are followed.

4. Results

4.1. Biostratigraphy of the Loho forearc basin

The Loho forearc basin in the middle Coastal Range is composed of the Lichi Mélange in the west and stratified flysch sequences (Takangkou Formation) of the remnant basin in the east (Fig. 4A). Stratified flysch sequences thrust westward over the Lichi Mélange along a low-angle thrust fault (Fig. 4B). Due to

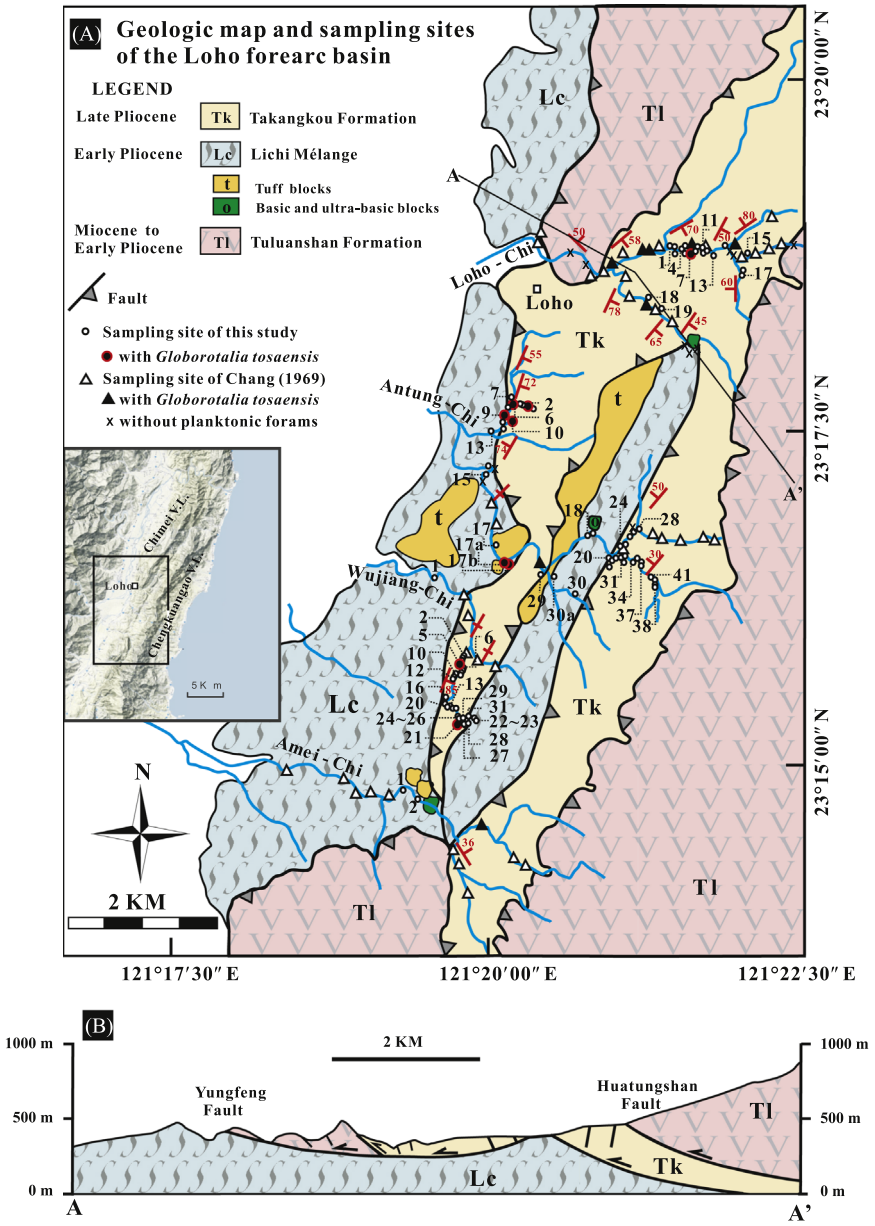

Fig. 4. (A) Geologic map and sampling sites of the Loho forearc basin (including the Lichi Mélange in the west and the Loho remnant forearc basin in the east) and (B) geologic cross section AA′. In Fig. 4A, inset shows topography of the middle Coastal Range and the location of this map. Both sampling sites in this study and Chang (1969) are shown. Part of the sample numbers in this study are also marked in this map, and the prefixes LH for Loho-Chi section, AT for Antung-Chi section, WJ for Wujiang-Chi section and AM for Amei-Chi section are omitted. See the related generalized lithologic columns in Fig. 5.

river erosion, the Lichi Mélange beneath the fault has been exposed in the remnant basin center as a window structure (Fig. 4A and B).

Eighty-one samples of the stratified flysch sequences and 15 samples of the sheared muddy matrix in the Lichi Mélange exposed along four river sections (from north to south: the Loho-Chi, Antung-Chi, Wujiang-Chi and Amei-Chi) are collected for microplankton study (Fig. 4A). In addition, previous study results of planktonic foraminifera in 41 samples collected from the Loho forearc basin (Chang, 1969) are included to improve age determinations (Figs. 4A and 5). Detail stratigraphic distributions of planktonic foraminifera and calcareous nannofossils are listed in Tables A1–A7 (see Appendix A).

In stratified flysch sequences, most samples are rich in well-preserved warm-water planktonic foraminifera of *Globigerinoides triloba* (Reuss), *Globigerinoides immaturus* Leroy, *Globigerinoides sacculifer* (Brady), *Globigerinoides ruber* (d'Orbigny), *Orbulina universa* d'Orbigny, *Globorotalia menardii* (Parker, Jones & Brady), *Globorotalia limbata* (Fornasini), *Globorotalia tumida* (Brady), *Globorotalia inflata* d'Orbigny, *Globorotalia crassaformis* (Galloway & Wissler), *Neogloboquadrina humerosa* (Takayanagi & Saito), *Pulleniatina obliquiloculata* (Parker & Jones) and *Sphaeroidinella dehiscens* (Parker & Jones). Some age-diagnostic species like *Globorotalia tosaensis* Takayanagi & Saito (FAD: 3.35 Ma), *Globigerinoides fistulosus* (Schubert) (FAD: 3.33 Ma) and *Globorotalia multicamerata* Cushman & Jarvis (LAD: 2.98 Ma) continuously or sporadically occur from the base of the stratified flysch sequences exposed in the studied sections (Fig. 5). Occurrence of this foraminiferal assemblage suggests that the stratified flysch sequences were deposited in lower Zone N21 (3.4–3.0 Ma). This foraminiferal assemblage is concurrent with the calcareous nannofossil assemblage of *Coccolithus pelagicus* (Wallich), *Calcidiscus leptoporus* (Murray & Blackman), *Calcidiscus macintyrei* (Bukry & Bramlette), *Discoaster brouweri* Tan, *Discoaster surculus* Martini & Bramlette (LAD: 2.49 Ma), *Helicosphaera sellii* Bukry & Bramlette, *Pseudoemiliania lacunosa* (Kamptner) (FAD: ~4.0 Ma; Gartner, 1990), *Reticulofenestra pseudo-*

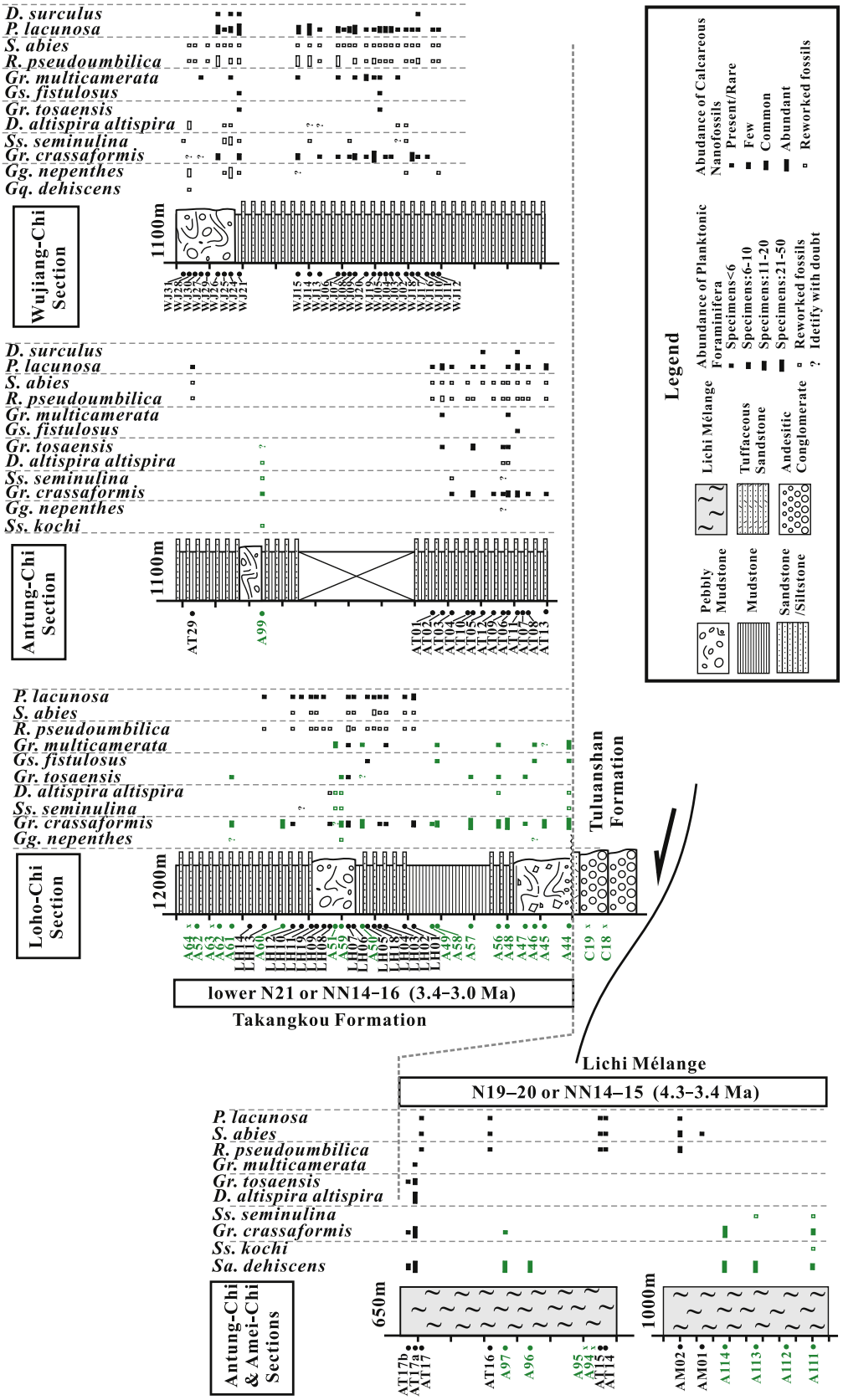

Fig. 5. General lithologic columns and distribution of microfossils of the Loho forearc basin. Only the Lichi Mélange and the normal sequences (Takangkou Formation) in the west rich in age-diagnostic fossils are presented. Samples derived from Chang (1969) in green are included to improve age determinations. Sampling sites without planktonic foraminifera are marked as cross. (For interpretation of the references to color in this figure legend, the reader is referred to the web version of this article.)

umbilica (Gartner), *Sphenolithus abies* Deflandre and *Sphenolithus moriformis* Brönnimann & Stradner. However, these nannofossils indicate a relatively wider age range (Zones NN14–16, ~4.0–2.5 Ma) than planktonic foraminifera.

Due to a turbidity transportation, stratified flysch sequences contain sporadic occurrences of ill-preserved, reworked planktonic foraminifera of *Globigerina nepenthes* Todd (LAD: 4.37 Ma), *Sphaeroidinellopsis seminulina* (Schwager) (LAD: 3.59 Ma), *Dentoglobigerina altispira altispira* (Cushman & Jarvis) (LAD: 3.47 Ma) and *Globoquadrina dehiscens* (Chapman, Parr & Collins) (FAD: 22.44 Ma; LAD: 5.92 Ma) mixing with the Late Pliocene assemblage (Fig. 5). Furthermore, they are abundant in the pebbly mudstone of debris flow deposits in the Wujiang-Chi section (Fig. 5). In addition, there are also reworked calcareous nannofossils of *R. pseudoumbilica* (LAD: 3.70 Ma), *S. abies* (LAD: 3.54 Ma), *S. moriformis* (NP11–NN8; Eocene–Late Miocene), *Sphenolithus heteromorphus* Deflandre (NN4–5; Middle Miocene) and *Cyclicargolithus floridanus* (Roth & Hay) (NP20–NN6; Late Eocene–Middle Miocene) in the Late Pliocene stratified flysch sequences (Fig. 5).

Muddy matrix in the Lichi Mélange contains *Sa. dehiscens* (FAD: 5.53 Ma) and *Gr. crassaformis* (FAD: 4.31 Ma) without *Gg. nepenthes* (LAD: 4.37 Ma), suggesting an age no older than 4.3 Ma. The youngest age can be determined by the concurrence of well-preserved *D. altispira altispira* (LAD: 3.47 Ma) and *Gr. tosaensis* (FAD: 3.35 Ma) at site AT17a of the Antung-Chi section (Figs. 4A and 5). As shown by these data, the Lichi Mélange is well fixed in Zones N19–20 (4.3–3.4 Ma). This age is consistent with occurrences of calcareous nannofossils of *P. lacunosa*, *R. pseudoumbilica* and *S. abies* of Zones NN14–15 (~4.0–3.7 Ma).

In conclusion, the Lichi Mélange in the west and stratified flysch sequences in the east are determined to be 4.3–3.4 Ma and 3.4–3.0 Ma in age, respectively (Fig. 5).

4.2. Biostratigraphy of the Taitung remnant forearc basin

Fieldwork and stratigraphic study on the Taitung remnant forearc basin are conducted mainly along three creek sections (from north to south: Chili-Chi, Tengchiao-Chi and Chunchieh-Chi) cross-cutting stratified flysch sequences (Fig. 6). Fifty-three samples of mudstone or siltstone are collected for study. The result is summarized in Fig. 7. Planktonic foraminifera and nannofossils identified in this study are listed in Tables B1–B6 (see Appendix B) in detail.

Like microfossils in the Loho remnant forearc basin to the north, most of the study samples of the Taitung remnant forearc basin are dominated by abundant warm-water fauna of *Gs. triloba*, *Gs. immaturus*, *Gs. sacculifer*, *Gs. ruber*, *Gr. menardii*, *Gr. tumida*, *Gr. inflata*, *Gr. crassaformis*, *N. humerosa*, *Pu. obliquiloculata*, *Sa. dehiscens* and *Globigerinita glutinata* (Egger). There are also age-diagnostic species of *Gr. tosaensis*, *Gr. limbata*, *Gr. multicamerata*, *Globorotalia ungulata* Bermúdez, *Globorotalia truncatulinoides* (d'Orbigny), *Gs. fistulosus* and *Globigerinoides extremus* Bolli & Bermúdez (Fig. 7). In addition, calcareous nannofossils of *P. lacunosa*, small *Gephyrocapsa* spp., *C. leptoporus*,

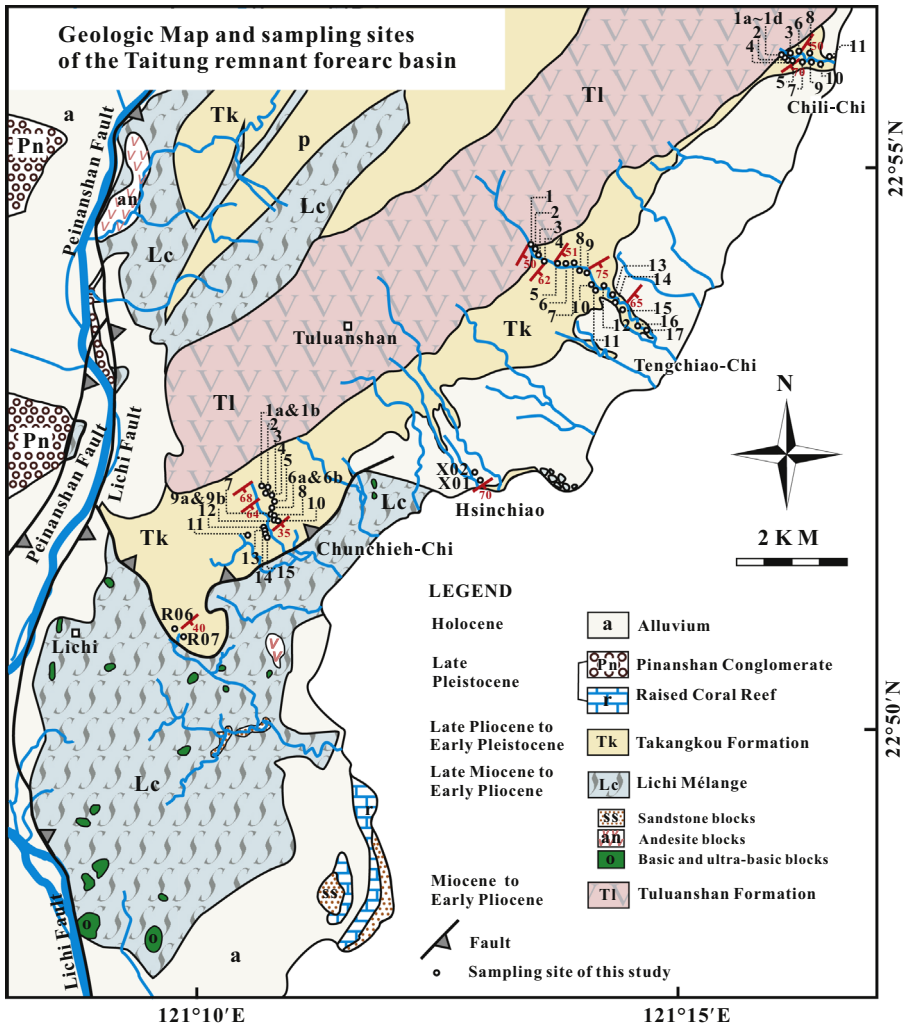

Fig. 6. Geological map and sampling sites of the Taitung remnant forearc basin (modified from Lin et al., 2008). All the sample numbers are presented, and the prefixes Q for Chili-Chi section, T for Tengchiao-Chi section and J for Chunchieh-Chi section are omitted. See the related generalized lithologic columns and sampling sites in Fig. 7.

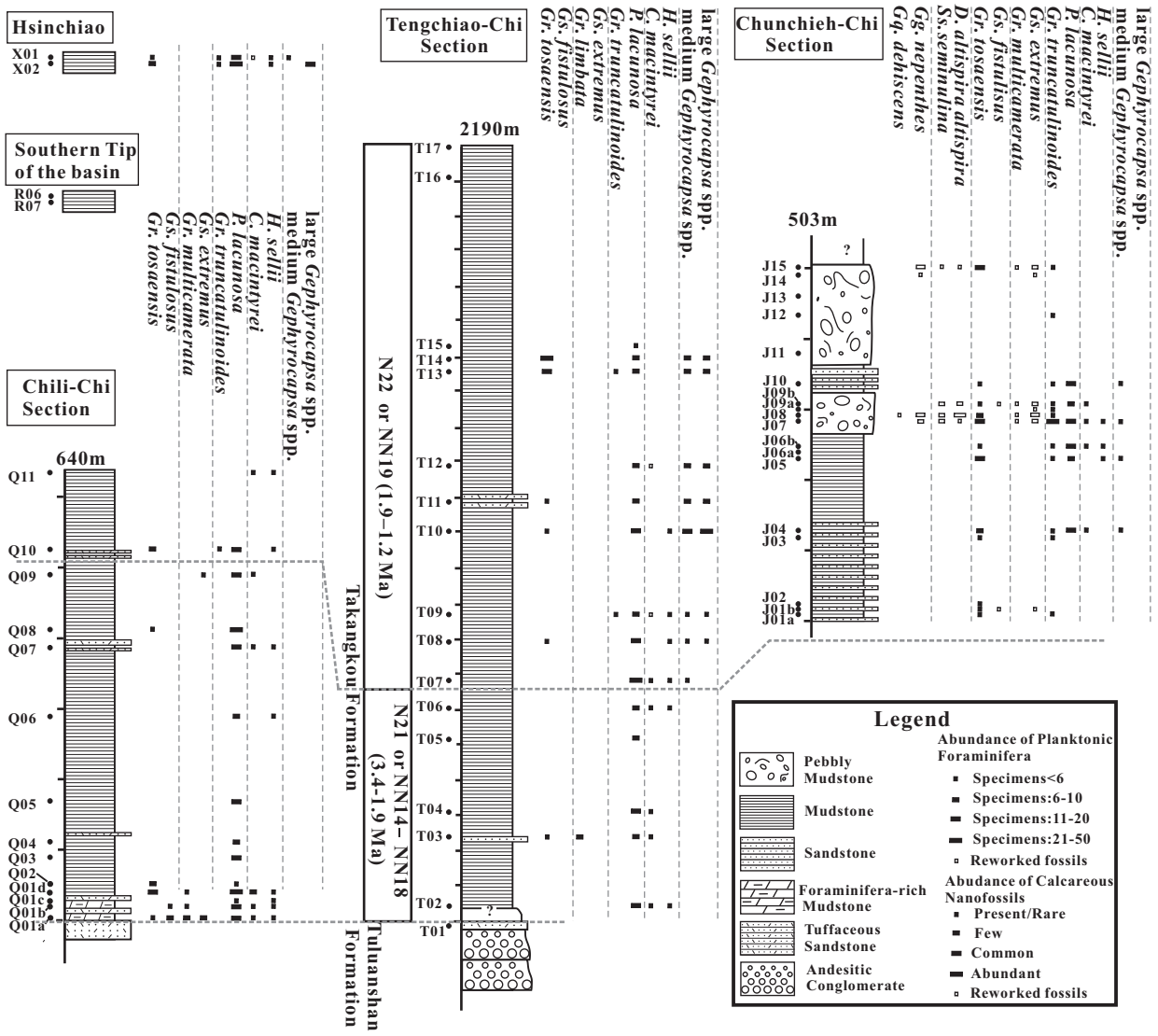

Fig. 7. General lithologic columns and distribution of microfossils of the Taitung remnant forearc basin.

Crenalithus doronicoides (Black & Barnes) and small *Coccolithus* sp. appear frequently in most of the samples. *H. sellii*, *C. macintyrei*, medium *Gephyrocapsa* spp. (over 4 μm) and large *Gephyrocapsa* spp. (over 5.5 μm) occur in minor numbers but are of great significance (Fig. 7). However, species of the genus *Discoaster* are rare.

The lower–middle part of the Chili-Chi section (sites Q01a–Q09) and the lower part of the Tengchiao-Chi section (sites T02–T06) yield age-diagnostic planktonic foraminifera of *Gr. tosaensis* (FAD: 3.35 Ma), *Gs. fistulosus* (FAD: 3.33 Ma), *Gr. ungulata* (N21–Recent) and *Gs. extremus* (LAD: 1.98 Ma), but lack *Gr. truncatulinoides* (FAD: 1.93 Ma). This foraminiferal assemblage suggests an age of Zone N21 (3.4–1.9 Ma) (Fig. 7). There are also calcareous nannofossils of *P. lacunosa* (FAD: ~4.0 Ma, Gartner, 1990), *H. sellii* (LAD: 1.34 Ma) and *C. macintyrei* (LAD: 1.60 Ma) (Fig. 7). Furthermore, medium *Gephyrocapsa* spp. (FAD: 1.67 Ma) is always absent. Thus, these parts of the studied sections can be assigned to Zones NN14–18 (~4.0–1.7 Ma), in agreement with the result obtained from planktonic foraminifera.

Planktonic foraminiferal assemblage of *Gr. truncatulinoides* (FAD: 1.93 Ma) and *Gr. tosaensis* (LAD: 0.61 Ma) is found in the upper part of the Chili-Chi section (sites Q10–Q11), the middle–upper part of the Tengchiao-Chi section (sites T07–T17), the whole Chunchieh-Chi section and supplementary sites at Hsinchiao of the highest stratigraphic position (Figs. 6 and 7), indicating an age of Zone N22 (1.9–0.6 Ma). Meanwhile, there are continuous occurrence of calcareous nannofossils of medium *Gephyrocapsa* spp. (FAD: 1.67 Ma) and large *Gephyrocapsa* spp. (FAD: 1.46 Ma; LAD: 1.24 Ma) (Fig. 7). Sequential appearance of *C. macintyrei* (LAD: 1.60 Ma) and *H. sellii* (LAD: 1.34 Ma) can be observed above site T09 in the Tengchiao-Chi section (Fig. 7). Thus, we can get an age of Zone NN19 (1.7–1.2 Ma), consistent with the result obtained from planktonic foraminifera.

Like the case in the Loho remnant forearc basin, abundant planktonic foraminifera indicative of Late Miocene–Pliocene concentrate in the pebbly mudstone in the Chunchieh-Chi section, such as *Gg. nepenthes*, *Globigerinoides obliquus* Bolli, *Gs. extremus*, *Globorotalia plesiotumida* Blow & Banner, *Gr. limbata*, *Gq. dehiscens*, *D. altispira altispira*, *Sphaeroidinellopsis subdehiscens* Blow, *Ss. seminulina* and *Sphaeroidinellopsis kochi* Caudri. They are interpreted as redeposited fossils due to the presence of considerable specimens of *Gr. truncatulinoides* (Fig. 7). However, reworked calcareous nannofossils of diverse ages, e.g. *R. pseudoumbilica* (LAD: 3.70 Ma), *S. abies* (LAD: 3.54 Ma), *S. moriformis* (NP11–NN8; Eocene–Late Miocene), *Discoaster quinqueramus* Gartner (NN11; Late Miocene), *C. floridanus* (NP20–NN6; Late Eocene–Middle Miocene) and *Dictyococcites hesslandii* (Haq) (NP18–NP24; Late Eocene–Early Oligocene), are scattered in the whole stratified flysch sequences.

Integrating both planktonic foraminifera and calcareous nannofossils provides robust age constraints for the stratified flysch sequences, ranging from 3.4 Ma to 1.2 Ma (Fig. 7).

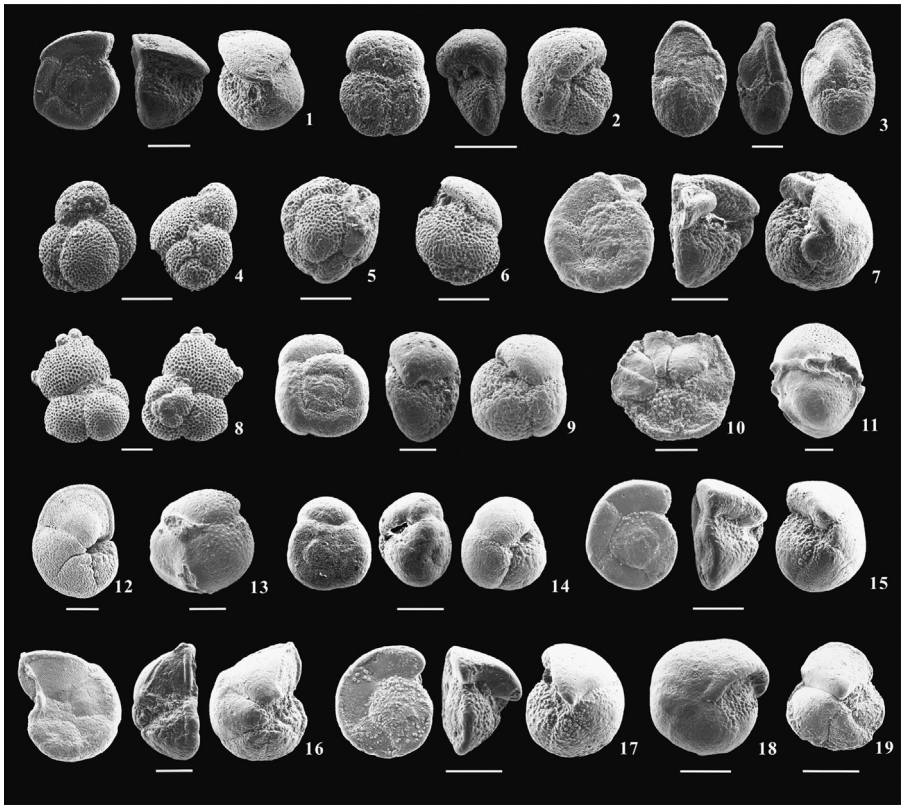

Fig. 8. SEM images of planktonic foraminifera recovered from the Loho forearc basin and the Taitung remnant forearc basin are shown in scale bars of 200 μm. 1–6, Recovered from site AT17a, the Lichi Mélange in the Loho forearc basin: 1. *Globorotalia tosaensis* Takayanagi & Saito; 2. *Globorotalia crassaformis* (Galloway & Wissler); 3. *Globorotalia tumida* (Brady); 4. *Globigerinoides extremus* Bolli & Bermúdez; 5–6. *Dentoglobigerina altispira altispira* (Cushman & Jarvis). 7–11, Recovered from the Takangkou Formation in the Loho forearc basin: 7. *Globorotalia tosaensis* Takayanagi & Saito, site AT10; 8. *Globigerinoides fistulosus* (Schubert), site WJ21; 9. *Globorotalia crassaformis* (Galloway & Wissler), site WJ21; 10. *Globorotalia multicamerata* Cushman & Jarvis, site WJ20; 11. *Sphaeroidinella dehiscens* (Parker & Jones), site WJ09. 12–19, Recovered from the Takangkou Formation in the Taitung remnant forearc basin: 12. *Globorotalia tumida* (Brady), site Q11; 13. *Sphaeroidinella dehiscens* (Parker & Jones), site J05; 14. *Globorotalia inflata* d'Orbigny, site J05; 15. *Globorotalia tosaensis* Takayanagi & Saito, site J07; 16–17. *Globorotalia truncatulinoides* d'Orbigny, site J07; 18. *Pulleniatina obliquiloculata* (Parker & Jones), site J07; 19. *Globorotalia ungulata* Bermúdez, site J07.

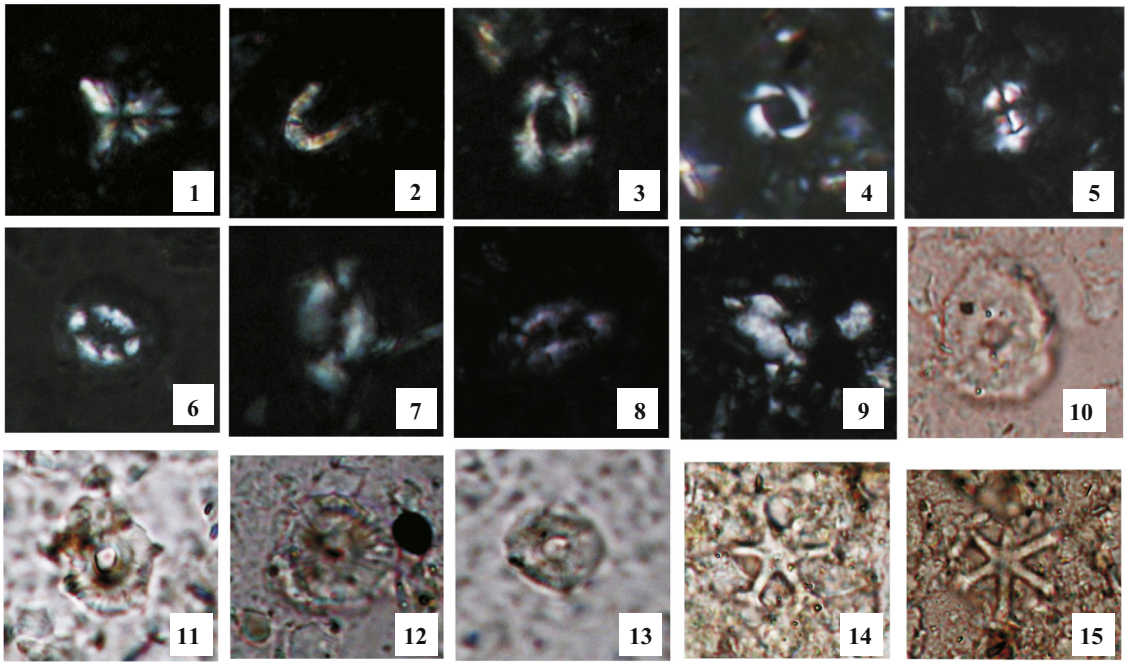

Fig. 9. Polarizing micrographs of calcareous nannofossils recovered from the Loho forearc basin. 1. *Sphenolithus abies* Deflandre, recovered from site WJ23, the Lichi Mélange. 2–15, Recovered from the Takangkou Formation: 2. *Ceratolithus rugosus* Bukry & Bramlette, site LH13; 3. *Reticulofenestra pseudoumbilica* (Gartner), site LH15; 4. *Pseudoemiliania lacunosa* (Kamptner), site LH15; 5–6. *Coccolithus pelagicus* (Wallich), site AT12; 7–9. *Helicosphaera sellii* Bukry & Bramlette, site WJ02; 10. *Calcidiscus macintyrei* (Bukry & Bramlette), site WJ06; 11–13. *Calcidiscus leptoporus* (Murray & Blackman), site LH07; 14. *Discoaster variabilis* Martini & Bramlette, site WJ24; 15. *Discoaster surculus* Martini & Bramlette, site WJ26.

5. Discussion

5.1. SCS long-term depleted deep-sea benthic foraminiferal $\delta^{13}C$ values responds to plate tectonics in the Taiwan region

Deep-water $\delta^{13}C$ variations in open oceans are controlled mainly by (1) changes in global carbon reservoirs that may result in carbon transfer among oceanic dissolved inorganic carbon, the terrestrial biomass and shelf sediments and(2) changes in global abyssal circulation, such as nutrient, ventilation, source, age and path of the bottom currents (Shackleton, 1977; Broecker, 1982; Miller and Fairbanks, 1985). Marginal seas like the SCS may differ from the open ocean due to variations in local surface productivity (Wei et al., 2006) and geographic isolation. For the latter, barriers may happen glacio-eustatically (Jian et al., 2003) or by local tectonics (e.g. Li et al., 2007).

The SCS rifted from the Eurasian Plate during Oligocene–Middle Miocene (Taylor and Hayes, 1983). Consequently, it is now surrounded by microcontinents: the Indochina Peninsula in the west, the South China continent in the north and the Borneo–Palawan–Mindoro microcontinent in the south. The SCS connects to the WP in the east through the Luzon Strait and to the Sulu Sea in the southeast through the Mindoro Strait (Fig. 1A; Wyrtki, 1961). The Luzon Strait (sill depth: ~2400 m) serves as the only channel for exchange of the deep water with the ocean outside, while the Mindoro Strait (sill depth: ~420 m) between Palawan and Mindoro only allows some exchange of intermediate water.

It should be noted that there might be a narrow deep-water gate between the Palawan–Mindoro block and the Philippine Mobile Belt in the Early to Middle Miocene (20–15 Ma) according to the paleogeographic reconstruction by Hall (2002). The SCS might connect to the Indian Ocean through this deep-water gate and then a series of marginal seas (the Proto-South China Sea, Sulu Sea, Celebes Sea and Molucca Sea). However, these marginal seas were separated from each other by volcanic arcs. It is difficult to value the deep connection between the SCS and the Indian Ocean. If the deep connection existed, it might be weak. Furthermore, the elimination of the Proto-SCS and the collision between the Palawan–Mindoro block and the Philippine Mobile Belt at ~15 Ma (Hall, 2002; Yumul et al., 2009) must have closed this connection. Therefore, we will neglect the deep connection between the SCS and the Indian Ocean in the following discussions. In contrast, since the generation of the SCS deep basin there has been a widely deep connection between the SCS and the WP through the Luzon Strait. At present, $\delta^{13}C$ of dissolved inorganic carbon of the WP bottom water below 2500 m (about 0‰) is higher than that of the SCS deep water at 2500 and 3000 m (about −0.2‰; Sheu et al., 1996; Chou et al., 2007), which might be an effect of the tectono-morphological barriers in the Luzon Strait.

To identify local factors controlling benthic $\delta^{13}C$ variations of the SCS in the past, we compare the Site 1148 benthic $\delta^{13}C$ curve with the Pacific composite benthic $\delta^{13}C$ record of Poore et al. (2006) (Fig. 10). Clearly the lower benthic $\delta^{13}C$ values after 16 Ma largely remain for the SCS, but its $\delta^{13}C$ curve fits better with the Pacific composite record than with the global (Figs. 2 and 10). It demonstrates that the SCS deep water is fed by the Pacific Ocean and implies that the long-term trend of the SCS deep-sea benthic $\delta^{13}C$ variations is primarily controlled by the Pacific abyssal circulation. Both records of the Pacific and the SCS show long-period excursions in $\delta^{13}C$ driven by changes in the global carbon reservoir (e.g. Miller and Fairbanks, 1985), such as the Early Miocene $\delta^{13}C$ positive excursion between 23 and 22 Ma, and the Monterey carbon excursion between 17.5 and 13.5 Ma (Fig. 10; Zhao et al., 2001; Wang et al., 2003; Poore et al., 2006). Most importantly, when compared to the Pacific composite record, the SCS benthic $\delta^{13}C$ record still clearly shows the particularly low values at 13.2, 10.5, 6.5,

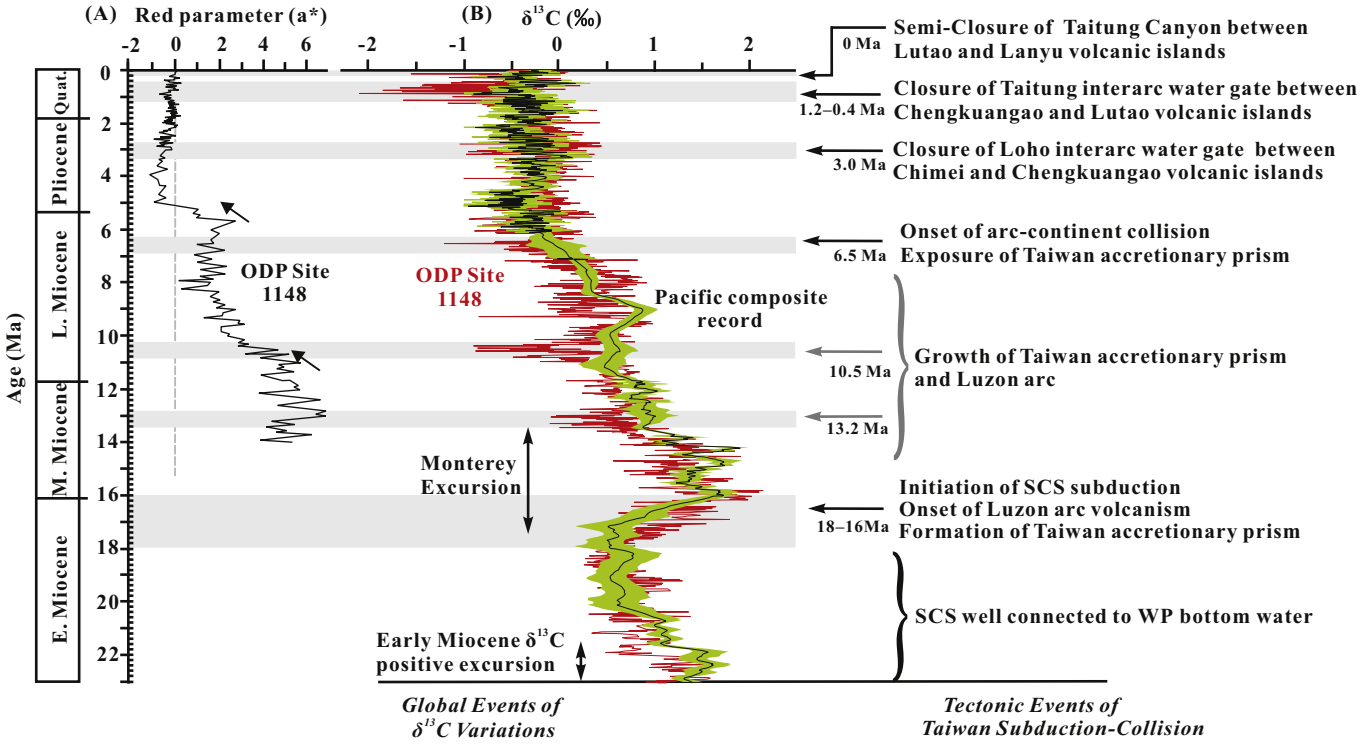

Fig. 10. (A) Variations of red parameter (a*) since 14 Ma at ODP Site 1148 (Li et al., 2007). Red parameter registers the relatively intensity of red color and green color of sediments, and the positive and negative values represent oxygen-rich and oxygen-poor waters, respectively (Li et al., 2007). (B) Comparison between benthic foraminiferal $\delta^{13}C$ at ODP Site 1148 (Tian et al., 2008) and the Pacific composite record (Poore et al., 2006). For the latter, a linear regression line in black with a 95% confidence band in light green (Poore et al., 2006) is shown. Also shown is the correlation between unusual depletion events of benthic $\delta^{13}C$ at ODP Site 1148 and tectonic events of Taiwan subduction–collision. (For interpretation of the references to color in this figure legend, the reader is referred to the web version of this article.)

3.0 and 1.2–0.4 Ma with offsets of 0.5–1.0‰, confirming the existing of local factors.

If the $\delta^{13}C$ depletion events are caused by local surface productivity, there should be contemporary enhancement events in surface productivity at Site 1148. However, except for high-productivity interval of the last 3 Ma indicated by an increased abundance of benthic foraminifera group and *Neogloboquadrina dutertrei* of high-productivity proxies (Zhao et al., 2009; Jian et al., 2003), no other high surface productivity events coeval to the $\delta^{13}C$ depletion events have been discerned. Accordingly, we infer that the isolation of the SCS from the Pacific is the main factor controlling the $\delta^{13}C$ depletion events. As the SCS is isolated progressively from the WP, its deep water would become stagnant and less ventilated, and accumulate more terrestrial organic materials. Deep-sea benthic $\delta^{13}C$ values would become much depleted (Li et al., 2007). Also, the dissolved oxygen content of the SCS deep sea water would decrease. It is evidenced by drops in the red parameter of the sediment color at Site 1148 at ~10.5 Ma and ~6 Ma, not returning to previous states (Fig. 10; Li et al., 2007). Glacio-eustatic variations in sill depth in the Luzon Strait of no more than 200 m may not make much difference to the deep SCS circulation. Consequently, the primary control of a long term trend of depleted $\delta^{13}C$ values in the SCS would be its semi-isolation by plate tectonics.

5.2. Initiation of the SCS subduction in the Middle Miocene (18–16 Ma) to develop two tectono-morphological barriers

Subduction of the SCS oceanic lithosphere beneath the NW-moving Huatung Basin/Philippine Sea Plate creates the Taiwan accretionary prism and the Luzon volcanic arc. Before the subduction, the SCS deep basin was much wider than the present state (Teng, 1990; Huang et al., 1997). The SCS could contact with the Philippine Sea Plate along a strike-slip fault (Teng, 1990; Hall, 2002) and the WP bottom water (below 2500 m) can easily exchange with the deep SCS. Therefore, the deep-sea benthic $\delta^{13}C$ values of the SCS are similar to the global and the Pacific composite records (Figs. 2 and 10).

The initiation of the SCS subduction can be understood by age dating on the infant Luzon arc–forearc basement and the earliest volcanism of the Luzon arc in the upper plate. Like the modern Mariana forearc (Bloomer et al., 1995), the Luzon arc–forearc basement is comprised of new supra-subduction zone (SSZ) lithosphere formed by forearc spreading in the extending upper plate during initiation of subduction. In the last 1 Ma, the Luzon arc–forearc thrust westward over the accretionary prism to form the Coastal Range. Ophiolitic blocks of the SSZ lithosphere were thus emplaced westward into the Huatung Ridge (deformed forearc sequences), generating the block-in-matrix Lichi Mélange in the Coastal Range (Huang et al., 2008). Age determinations on zircon grains in isotropic gabbro and plagiogranite blocks gave 16.86 ± 0.27 Ma and 17.7 ± 1.47 Ma, respectively (Huang et al. (unpublished results)). Hence, the age of the infant Luzon arc–forearc basement can be constrained in 18–16 Ma. This age is supported by calcareous nannofossils in red shale inserted between pillow lava of SSZ blocks (Zone NN5, 14.9–13.3 Ma; Huang et al., 1979). On the other hand, both fission track and $^{40}Ar/^{39}Ar$ dating for the oldest volcanic sequence exposed on the Coastal Range gave an age of ~16 Ma (Yang et al., 1988, 1995; Lo et al., 1994). Accordingly, the earliest volcanism of the Luzon arc is around 16 Ma. All these results suggest that the initiation of the SCS lithosphere subduction occurred in the Middle Miocene (18–16 Ma).

From the initiation of the SCS subduction to the onset of arc–continent collision (~6.5 Ma), active volcanism has gradually built the bathymetric high of the Luzon arc on the Huatung Basin floor. Consistent with a southward propagation of the arc–continent collision, the volcanism ceased sequentially from north to south: 6–5 Ma for the Chimei volcanic island, 3.3 Ma for the Chengkuangao volcanic island, and 1.5–0.02 Ma for the offshore Lutao–Lanyu volcanic islands, respectively (Lo et al., 1994; Yang et al., 1995; Huang et al., 2006). It is still active at present in the Batan–Babuyan volcanic islands. On the other hand, during the subduction, slope sediments on the Asian passive margin are progressively scraped off and accreted eastward to the frontal Taiwan accretionary prism.

Thus, the deep-sea benthic $\delta^{13}C$ values of the SCS began to diverge from the global and the Pacific composite records to lighter values since ~16 Ma (Figs. 2 and 10). Significant $\delta^{13}C$ depletion events at 13.2 Ma and 10.5 Ma (along with the decrease in the red parameter) might imply major eruption events of the Luzon arc (Fig. 10). They would dramatically raise the height of the volcanic edifice and further weaken or close the WP bottom-water connection to the deep SCS.

5.3. Exposing the Taiwan accretionary prism since ~6.5 Ma narrowed the WP–SCS gateway

When the Taiwan accretionary prism (now ~400 km long) was exposed from north to south to sub-aerial erosions, the width of the Luzon Strait water gateway between the SCS and the WP would have been shut down progressively for hundreds of kilometers. Consequently, water exchange, not only deep water but also intermediate and surface water, between the WP and the SCS would differ from what happened before and the SCS would be more isolated from the open WP. The exposed Taiwan accretionary prism (now the Central Range–Hengchun Peninsula; Fig. 1C) becomes the source for orogenic clastics supplied westward to the foreland basin and eastward to the forearc basin (Fig. 1C). Therefore, the stratigraphy of the foreland basin in the Taiwan Strait–Coastal Plain–Western Foothills and the forearc sequences in the Coastal Range can be used to date the exposure event of the Taiwan accretionary prism.

In the Taiwan Strait–Coastal Plain–Western Foothills, the Taiwan-sourced Latest Miocene–Pleistocene foreland sequences dip to the west and lap westward upon the east-dipping, continent-derived, shallow-marine strata of Early–Middle Miocene age. Between them is an unconformity or depositional hiatus representing the base of the foreland basin (Lin et al., 2003). Seismic surveys over the Taiwan Strait–Coastal Plain and the reconstructed stratigraphy in the Western Foothills show that sedimentation of the foreland sequences starts from ~6.5 Ma in the north and at ~4.4 Ma in the south (Lin et al., 2003; Yang et al., 2014).

Forearc sequences in the Coastal Range include the Lichi Mélange in the west and stratified remnant forearc sequences in the east (Huang et al., 2008). Detailed reconstruction of forearc stratigraphy reveals that the oldest forearc sediments sourced from the accretionary prism are always found in the Lichi Mélange (~6.6 Ma; Chen et al., unpublished results). They are coeval with the oldest strata in the foreland basin (~6.5 Ma; Lin et al., 2003). These oldest forearc sediments are preserved in limit outcrops in the southern Coastal Range. However, only younger forearc sediments (4.3–3.4 Ma) are found in the Lichi Mélange west of the Loho forearc basin in the middle Coastal Range (see Section 4.1).

The exposure event of the accretionary prism can be also constrained by the stratigraphy of the slope basin unconformable on the deformed accretionary prism in the Hengchun Peninsula. These shallow-marine slope basin sediments are derived from the exposed accretionary prism to the north (Huang et al., 2006). Planktonic foraminiferal assemblage recovered from the basal part of the slope basin (Maanshan Formation in the West Hengchun Hill) suggests an age of 4.3–3.6 Ma (Early Pliocene; Cheng and Huang, 1975; Huang et al., 2006), consistent with the onset of foreland sedimentation in the southern part of the Western Foothills (Yang et al., 2014).

In conclusion, independent studies on the foreland basin, forearc basin and slope basin indicate the accretionary prism of the Central Range being exposed sub-aerially to erosion since ~6.5 Ma. Since then the width of the Luzon Strait between the WP

and the SCS has been narrowed progressively for hundreds of kilometers. The SCS has been further isolated from the open WP. Hence the benthic $\delta^{13}C$ depletion event at 6.5 Ma and the sharp decline in oxygen levels (Fig. 10).

5.4. Closures of interarc water gates

5.4.1. Semi-closure of the modern interarc water gate between the Lutao and Lanyu volcanic islands in the incipient arc–continent collision zone off SE Taiwan

The WP deep water intrudes westward through the interarc water gates of the Taitung Canyon (0.4 Sv) and the Bashi Channel (1.2 Sv), and then detours southward along the North Luzon Trough to enter the deep SCS (Fig. 1B). At present, the Taitung Canyon also serves as the main active conduit transporting Taiwan-sourced orogenic sediments eastward to the Huatung Basin east of the Luzon arc (Schnűrle et al., 1998). However, the WP deep water intrudes into the SCS mainly through the shallow Bashi Channel (~2400 m) instead of the deep Taitung Canyon (~3000 m). This suggests that the sill depth of the interarc water gates is not the main factor controlling the principal path of the westward-intruding WP deep water.

Instead, the variation of the WP deep water flux through the interarc water gates depends on deformations in the North Luzon Trough forearc basin. Bathymetric surveys and seismic investigations in the modern subduction–collision zone off SE Taiwan show that forearc strata in the active collision zone north of 21°20′N are backthrust arcward and thus uplifted on the order of km to develop the Huatung Ridge (with crest less than 1000 m depth) above the remnant forearc basin in the east (Fig. 1B and C; Reed et al., 1992; Chang et al., 2001). In addition, due to a southward propagation of the oblique arc–continent collision, diachronic clockwise rotation of the volcanic islands in different tectonic zones may further complicate the forearc deformation (Huang et al., 1992). Now the Lutao volcanic island has clockwise rotated for 14°, but the Lanyu volcanic island in the subduction zone is not rotated yet (Figs. 1C and 11D; Yang et al., 1983). This would create a left-lateral strike-slip fault running along the Taitung Canyon (Schnűrle et al., 1998; Kao and Huang, 2000).

Because of both the eastward propagation of backthrusting and the strike-slip fault, remnant forearc sequences south of the strike-slip fault and west of the Lanyu volcanic island are also deformed and uplifted as part of the Huatung Ridge, i.e. the HTWL with sill depth of ~2300 m (Figs. 1C and 11D). The HTWL connecting northeastward to the Taitung Canyon is thus semi-closed. In contrast, no intensive deformation of forearc strata occurs in the subduction zone south of 21°N (Figs. 1 and 11D). Consequently, the North Luzon Trough in the subduction zone is open, wide and deep (~3500 m), and the Bashi Channel–North Luzon Trough becomes the main route for the WP intruding into the deep SCS. Meanwhile the Taitung Canyon–HTWL in the active collision zone can only serve as a subordinate route (Figs. 1 and 11D).

5.4.2. Closures of the Loho interarc water gate and the Taitung interarc water gate at ~3.0 Ma and ~1.2 Ma, respectively

Due to a southward propagation of the oblique arc–continent collision, modern tectonic processes operating off SE Taiwan spatially are analogous to what happened before formation of the Coastal Range.

Compared to modern marine geology in the incipient arc–continent collision zone off SE Taiwan, the Lichi Mélange in the Coastal Range (Fig. 3) represents the early backthrusting Huatung Ridge in the west, while the normal flysch sequences mark the deposition in the remnant forearc basin in the east during the active arc–continent collision in Plio-Pleistocene time. Previous study showed that both the Lichi Mélange and the normal flysch sequences yield indigenous deep-marine benthic foraminifers living in water depths of 1500–3000 m similar to the modern North Luzon Trough (Chang, 1967; Huang et al., 2008). Among four remnant forearc basins in the Coastal Range, the Loho and the Taitung remnant forearc basins are characterized by their special positions connecting to the interarc passage between volcanic islands (Fig. 3), similar to the HTWL off SE Taiwan.

Consequently, the youngest strata of the Loho and the Taitung remnant forearc basins delineate the time when they were uplifted to be incorporated into the late deformed Huatung Ridge. Once the Loho and the Taitung remnant forearc basins were deformed, uplifted and thus closed, the Loho and the Taitung interarc water gates would be also closed to the WP deep water. Integrated biostratigraphy of both planktonic foraminifera and calcareous nannofossils in the Loho and the Taitung remnant forearc basins shows ages of 3.4–3.0 Ma and 3.4–1.2 Ma, indicating that they were deformed, uplifted and closed at ~3.0 Ma and ~1.2 Ma, respectively (Fig. 11B and C). This implies that the North Luzon Trough has been semi-closed progressively from north to south: ~3.0 Ma in the Loho interarc water gate between the Chimei and Chengkuangao volcanic islands, ~1.2 Ma in the Taitung interarc water gate between the Chengkuangao and Lutao volcanic islands, and presently in the Taitung Canyon between the Lutao and Lanyu volcanic islands (Fig. 11). These closure events are simultaneous with diachronic clockwise rotation of volcanic islands due to a propagation of the oblique arc–continent collision (4–3 Ma in the Chimei volcanic island; 2–1 Ma in the Chengkuangao volcanic island; and presently in the Lutao volcanic island; Yang et al., 1983; Lee et al., 1991; Huang et al., 1992). The closure events also coincide with depleted deep-sea benthic $\delta^{13}C$ events at 3.0 and 1.2–0.4 Ma in the SCS (Fig. 10), and they show that fewer interarc passages can be used as routes for the WP deep water overflow (Fig. 11) and thus the deep SCS becomes more and more isolated from the open WP.

Following the closure of the Taitung interarc water gate, the Luzon arc–forearc was obducted westward onto the Central Range accretionary prism to form the Coastal Range. The sedimentation in the Suilien and the Taiyuan remnant forearc basins and the Chengkung intra-arc basin ceased during 1.2–0.8 Ma (Fig. 3; Chi et al., 1981; Horng and Shea, 1996; Huang et al., 1995). It indicates regional uplifting of the Luzon arc–forearc, which might also contribute to the remarkable depleted $\delta^{13}C$ event at 1.2–0.4 Ma. In addition, as indicated by the sudden decline of the Pacific bottom water markers of *Nuttallides umboniferous* (in >3000 m assemblage) at 1.2 Ma and *Favocassidulina favus* (in 3000–2500 m assemblage) since ~1.0–0.9 Ma at Site 1148 (Li et al., 2007, 2008), the tectonic events occurring in the Luzon arc–forearc since ~1.2 Ma had totally closed the connection of the SCS with the WP bottom water below 2500 m.

6. Conclusion

The deep-sea paleoceanographic history of the SCS is firmly linked to the tectonic evolution in the Taiwan Island–Luzon Strait region where the WP deep water enters the SCS. Results of previous and present study onshore and offshore Taiwan Island date tectonic events of (1) the initiation of the SCS subduction in 18–16 Ma, (2) the subaerial exposures of the Taiwan accretionary prism at ~6.5 Ma, and (3) the closures of the Loho and the Taitung interarc water gates between volcanic islands at ~3.0 and ~1.2 Ma respectively. These tectonic events coincide with the very low value events of deep-sea benthic foraminiferal $\delta^{13}C$ record in the SCS relative to the global and the Pacific composite records (Figs. 2 and 10).

The initiation of the SCS subduction beneath the Philippine Sea Plate since the Middle Miocene progressively builds the Taiwan accretionary prism and the Luzon arc. As these two tectono-morphographic barriers between the WP and the SCS grow, the WP bottom water can no longer invade the SCS as easily as before. This began a long-term trend of depleted deep-sea benthic $\delta^{13}C$ values in the SCS, lower than the Pacific and the global composite records

since 16 Ma. The emergence of the Taiwan accretionary prism since arc–continent collision at ~6.5 Ma further narrowed the Luzon Strait between the WP and the SCS by 400 km and caused further isolation of the SCS from the WP.

Interarc water gates connecting to the North Luzon Trough forearc basin are the main entrances for the WP deep water flowing into the SCS. Syn-collisional deformation of both eastward-migrated backthrusting and diachronic rotation between volcanic islands formed the Huatung Ridge in the North Luzon Trough, and this is critical to closures of the interarc water gates. As the arc–continent collision propagates southward since ~6.5 Ma, the closure process occurred progressively from north to south: 3.0 Ma in the Loho interarc water gate, 1.2 Ma in the Taitung interarc water gate, and presently in the Taitung Canyon (Fig. 11). Therefore, these water gates were sequentially closed to the WP deep water, and the SCS is semi-isolated today. The paleoceanographic outcome for the SCS has been long-term depletion (over 16 Ma) in deep-sea benthic foraminiferal $\delta^{13}C$ values, especially at 13.2, 10.5, 6.5, 3.0 and 1.2–0.4 Ma.

Acknowledgments

We thank Dr. Chih-Wei Chien for his help in the fieldwork and Dr. Wen-Rong Chi for his assistance in identifying the calcareous nannofossils. We also appreciate helpful discussion from Dr. Zhimin Jian. Critical reviews and constructed comments by Dr. Brian McGowran, Dr. Qianyu Li and an anonymous reviewer are greatly appreciated and significantly improved the paper. This work was financially co-supported by the National Natural Science Foundation of China (Grants 91128211 and 41176041), the Knowledge Innovation Program of the Chinese Academy of Sciences (Grant KZCX2-EW-101) and the Key Laboratory of Marine

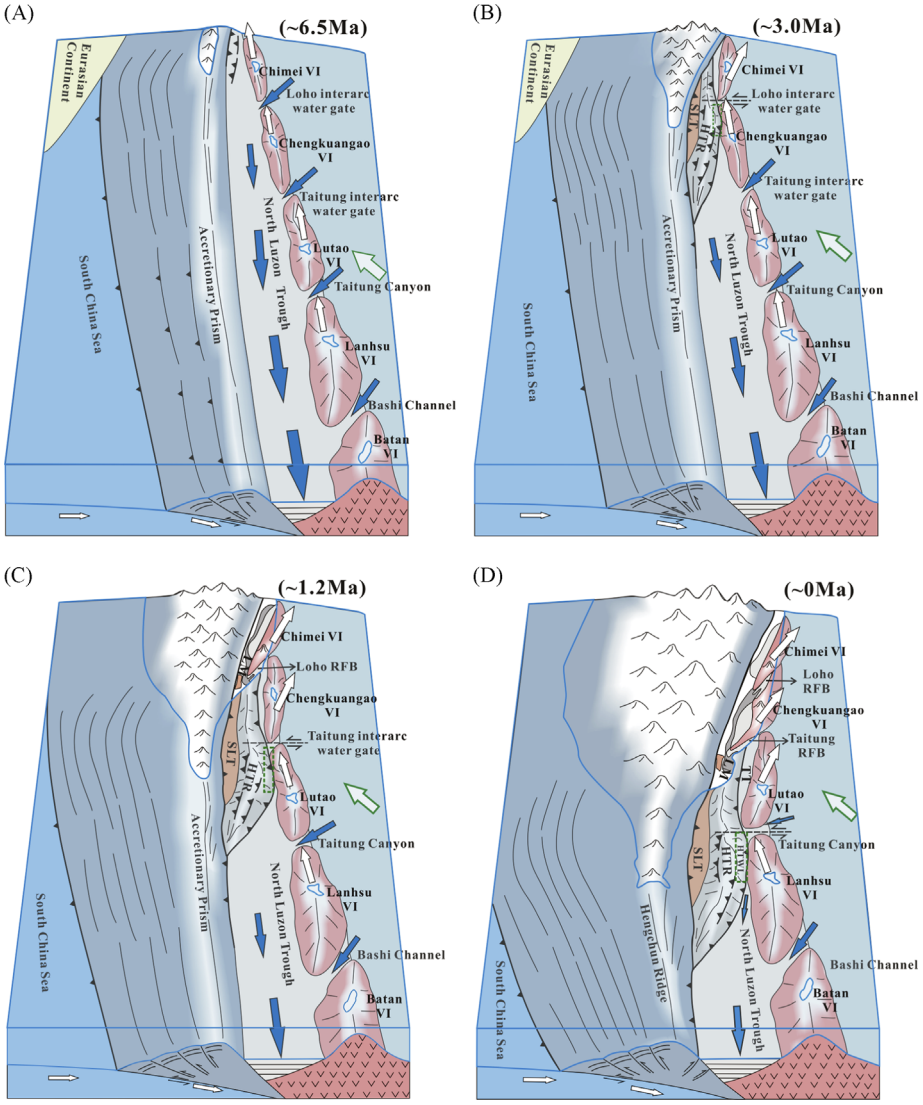

Fig. 11. Spatial and temporal evolution of interarc water gates between volcanic islands since ~6.5 Ma. (A) Westward thrust along the accretionary prism–forearc basin boundary and eastward backthrust began to develop the Huatung Ridge in the western part of the North Luzon Trough forearc basin at 6.5 Ma, but there is no significant deformation in the forearc basin connecting to the interarc water gates. (B) Closure of the Loho interarc water gate at ~3.0 Ma. (C) Closure of the Taitung interarc water gate at ~1.2 Ma. (D) Semi-closure of the Taitung Canyon at present. Green dashed rectangles in B–D show the paleogeographic location of the Loho remnant forearc basin, the Taitung remnant forearc basin and the HTWL, respectively. White arrows represent the paleomagnetic declination and diachronic rotation of the volcanic islands. Blue arrows show water transport from the West Pacific to the South China Sea. VI=volcanic islands; RFB=remnant forearc basin; HTR=Huatung Ridge; HTWL=late deformed Huatung Ridge west of the Lanyu VI; TT=Taitung Trough remnant forearc basin; SLT=Southern Longitudinal Trough. (For interpretation of the references to color in this figure legend, the reader is referred to the web version of this article.)

Hydrocarbon Resources and Environmental Geology, Ministry of Land and Resources (MRE201307). This is contribution No. IS-2043 from GIGCAS.

Appendix A

Check-list of microfossils identified in the Loho forearc basin (this study and Chang, 1969). Including 7 Tables A1–A7.

Table A1
Check-list of planktonic foraminifera identified in the Loho-Chi section.

Study section	Loho-Chi section											
Sample number	LH01	LH03	LH04	LH05	LH06	LH07	LH08	LH09	LH10	LH11	LH12	LH13
Stratigraphic unit	TK	TK	TK	TK	TK	TK	TK	TK	TK	TK	TK	TK
Globigerina bulloides d'Orbigny	1											
Globigerina parabulloides Blow												
Globigerina falconensis Blow												
Globigerina woodi Jenkins												
Globigerina nepenthes Todd												
Globigerina decoraperta Takayanagi & Saito												1
Globigerina rubescens Hofker												
Globigerinoides triloba (Reuss)	20	40	48	29	9	16	31	24	1	1	9	3
Globigerinoides immaturus Leroy	21	6	5	14	3	3	22	24	3	2	7	1
Globigerinoides sacculifer (Brady)	18	22	34	16		18	19	28			8	6
Globigerinoides fistulosus (Schubert)				2?								
Globigerinoides obliquus Bolli												
Globigerinoides extremus Bolli & Bermúdez	1					2	1					
Globigerinoides bollii Blow												
Globigerinoides conglobatus (Brady)	9		4	3		3	2	12		2	3	
Globigerinoides ruber (d'Orbigny)	20	6	15	24	4	62	48	40	5	5	7	9
Orbulina suturalis Brönnimann												
Orbulina universa d'Orbigny	10	1	7	4		8		18			4	4
Orbulina bilobata (d'Orbigny)												
Globorotalia menardii (Parker, Jones & Brady)	21	5	3	12	1	8		7	2		3	
Globorotalia limbata (Fornasini)	2					5						
Globorotalia multicamerata Cushman & Jarvis		1				4						
Globorotalia plesiotumida Blow & Banner												
Globorotalia tumida (Brady)		4		14	2	8	2	1			4	
Globorotalia flexuosa (Koch)	4											
Globorotalia ungulata Bermúdez												
Globorotalia scitula (Brady)	1	1						1				
Globorotalia conoidea Walters												
Globoratalia conomiozea Kennett												
Globorotalia inflata d'Orbigny	21	9	20	14		12	3	4			26	7
Globorotalia crassaformis (Galloway & Wissler)	7		2	4		9	2				1	
Globorotalia crassula Cushman & Stewart	1											
Globorotalia tosaensis Takayanagi & Saito						4						
Globoquadrina venezuelana (Hedberg)												
Globoquadrina dehiscens (Chapman, Parr & Collins)												
Globoquadrina baroemoenensis (LeRoy)												
Dentoglobigerina altispira altispira (Cushman & Jarvis)							1					
Neogloboquadrina acostaensis (Blow)												
Neogloboquadrina humerosa (Takayanagi & Saito)	32	27	50	64	7	18	68	67	12	8	104	41
Pulleniatina primalis Banner & Blow												
Pulleniatina obliquiloculata (Parker & Jones)	11	18	7				28	41	4	3	2	
Sphaeroidinellolsis seminulina (Schwager)									2?			
Sphaeroidinellolsis seminulina (Schwager) (immature form)												
Sphaeroidinellolsis subdehiscens Blow												
Sphaeroidinellolsis subdehiscens Blow (immature form)		1		3				2	1		3	
Sphaeroidinella dehiscens (Parker & Jones)	35	7	46	21	16	6	8	21	12		46	34
Globigerinita glutinata (Egger)	4		1	2		17	2	2	1	1		
Globigerinella obesa (Bolli)								1?				
Globigerinella aequilateralis (Brady)												
Globigerinella calida (Parker)												
Candeina nitida d'Orbigny												
Total number	239	148	242	226	42	203	237	293	43	23	227	106

Notes: TK=Takangkou Formation (mudstone); p.m.=Takangkou Formation (pebbly mudstone); LC=Lichi Mélange (muddy matrix).

Table A2
Check-list of calcareous nannofossils identified in the Loho-Chi section.

Study Section	Loho-Chi section																		
Sample Number Stratigraphic Unit	LH01 TK	LH02 TK	LH03 TK	LH04 TK	LH05 TK	LH06 TK	LH07 TK	LH08 TK	LH09 TK	LH10 TK	LH11 TK	LH12 TK	LH13 TK	LH14 TK	LH15 TK	LH16 TK	LH17 TK	LH18 TK	LH19 TK
Amaurolithus tricorniculatus (Gartner)			P								P								
Coccolithus miopelagicus Bukry																			
Coccolithus *pelagicus* (Wallich)	R	R		R	P	R	F		R		P	R	R				R	F	
Calcidiscus leptoporus (Murray & Blackman)	R		P			P	R		R		R	P	P					R	
Calcidiscus macintyrei (Bukry & Bramlette)	R	P	R				P		P	P	R			P			R		
Ceratolithus acutus Gartner & Bukry																			
Ceratolithus rugosus Bukry & Bramlette								P					P						
Cyclicargolithus floridanus (Roth & Hay)												P							
Discoaster asymmetricus Gartner									P										
Discoaster brouweri Tan			P				P			P							P		P
Discoaster pentaradiatus Tan	P																		
Discoaster quinqueramus Gartner												P							
Discoaster variabilis Martini & Bramlette						P													P
Gephyrocapsa spp. (small)		R	P	P	F		P	P	F								R	F	
Gephyrocapsa oceanica Kamptner (medium)																			
Helicosphaera ampliaperta Bramlette & Wilcoxon																			
Helicosphaera carteri (Wallich)																		P	
Helicosphaera sellii Bukry & Bramlette	R		P	P		R	R		R		P						P	R	
Pseudoemiliania lacunosa (Kamptner)	F	R	R	R	R	R	P		R	P	R	R	R					R	R
Reticulofenestra pseudoumbilica (Gartner)	R	R	R	R	R	R	F	R	R		R	R	R				R	R	R
Sphenolithus abies Deflandre	R	P	P	R		R	P				R	P					C	F	R
Sphenolithus heteromorphus Deflandre									P										
Sphenolithus moriformis Brönnimann &Stradner			P	R					P	P	R						A	R	

Notes for abundance: A=abundant; C=common; F=few; R=rare; P=present.

Table A3
Check-list of planktonic foraminifera identified in the Antung-Chi section.

Study section	Antung-Chi section																
Sample number	AT01	AT02	AT03	AT04	AT05	AT06	AT07	AT08	AT09	AT10	AT11	AT12	AT13	AT14	AT15	AT17a	AT17b
Stratigraphic unit	TK	TK	TK	TK	TK	TK	TK	TK	TK	TK	TK	TK	TK	LC	LC	LC	LC
Globigerina bulloides d'Orbigny									2			1					
Globigerina parabulloides Blow						1											
Globigerina falconensis Blow										3			1				
Globigerina woodi Jenkins																	
Globigerina nepenthes Todd									3?								
Globigerina decoraperta Takayanagi & Saito										1			1				
Globigerina rubescens Hofker	1	1				2						4					
Globigerinoides triloba (Reuss)		3	4			21		25	49	25	22	21	30			43	21
Globigerinoides immaturus Leroy		1	1			14		7	19	14	20	5	6			25	7
Globigerinoides sacculifer (Brady)		1	1			25		7	24	12	24	22	29			21	3
Globigerinoides fistulosus (Schubert)											1						
Globigerinoides obliquus Bolli									6				1				
Globigerinoides extremus Bolli & Bermúdez			2			3		2	2	2	2	5	4			16	
Globigerinoides bollii Blow									1								
Globigerinoides conglobatus (Brady)		2				5		1	1	13	23	3	4			16	
Globigerinoides ruber (d'Orbigny)		18	13			50		38	32	72	50	72	72			55	8
Orbulina suturalis Brönnimann									2		2						
Orbulina universa d'Orbigny		2				11		11	2	8	29	13	13			30	3
Orbulina bilobata (d'Orbigny)												1					
Globorotalia menardii (Parker, Jones & Brady)		1				15		5	3	8	22	30	24			10	
Globorotalia limbata (Fornasini)		3				6		6	3	20	8	11	2			11	5
Globorotalia multicamerata Cushman & Jarvis		1				1										1	
Globorotalia plesiotumida Blow & Banner									1?								
Globorotalia tumida (Brady)		2	1			5				1	12	12	1			25	5
Globorotalia flexuosa (Koch)																8	
Globorotalia ungulata Bermúdez												1				1	
Globorotalia scitula (Brady)													2			1	
Globorotalia conoidea Walters																	
Globoratalia conomiozea Kennett																	
Globorotalia inflata d'Orbigny																2	5
Globorotalia crassaformis (Galloway & Wissler)			2			7		2	2	6	7	2	2			23	2
Globorotalia crassula Cushman and Stewart																	
Globorotalia tosaensis Takayanagi & Saito		1				5			2	6						7	1
Globoquadrina venezuelana (Hedberg)																	
Globoquadrina dehiscens (Chapman, Parr & Collins)																	
Globoquadrina baroemoenensis (LeRoy)									1?								
Dentoglobigerina altispira altispira (Cushman & Jarvis)						1			2							36	
Neogloboquadrina acostaensis (Blow)																2	
Neogloboquadrina humerosa (Takayanagi & Saito)		3	4			73		7	8	38	42	46	18			17	15
Pulleniatina primalis Banner & Blow																	
Pulleniatina obliquiloculata (Parker & Jones)		3				1		5	13	12	1	11	2				
Sphaeroidinellolsis seminulina (Schwager)			1														
Sphaeroidinellolsis seminulina (Schwager) (immature form)									1								
Sphaeroidinellolsis subdehiscens Blow		1				3				2							
Sphaeroidinellolsis subdehiscens Blow (immature form)											1	3	1			1	
Sphaeroidinella dehiscens (Parker & Jones)			2			40		1	4	36	26	29	5			40	6
Globigerinita glutinata (Egger)			14					3				3	2				1
Globigerinella obesa (Bolli)						1				1			2			1?	
Globigerinella aequilateralis (Brady)		1				3				2	3	8	11			2	
Globigerinella calida (Parker)		1								1						1?	
Candeina nitida d'Orbigny																	
Total number	1	45	45			293		120	183	283	295	303	233			395	82

Study section	Antung-Chi section																	
Sample number	AT18	AT19	AT20	AT22	AT24	AT27	AT28	AT30a	AT31	AT32	AT33	AT34	AT35	AT36	AT37	AT38	AT39	AT40
Stratigraphic unit	LC	LC	TK	TK	TK	TK	TK	LC	TK	TK	TK	TK	TK	TK	TK	TK	TK	TK
Globigerina bulloides d'Orbigny																		
Globigerina parabulloides Blow					3													
Globigerina falconensis Blow																		
Globigerina woodi Jenkins																		
Globigerina nepenthes Todd					1?				1									
Globigerina decoraperta Takayanagi & Saito					1						1						1	
Globigerina rubescens Hofker					1													
Globigerinoides triloba (Reuss)				3	31	3			28	3	18	1	29	4	22	3	2	
Globigerinoides immaturus Leroy				6	9				19		1		7		11		1	2
Globigerinoides sacculifer (Brady)				6	7	7			6		2		15	2	110	7	1	1
Globigerinoides fistulosus (Schubert)																		
Globigerinoides obliquus Bolli																		
Globigerinoides extremus Bolli & Bermúdez					1				1									
Globigerinoides bollii Blow									5									
Globigerinoides conglobatus (Brady)					1	1			4	2	2		2		2		1	3
Globigerinoides ruber (d'Orbigny)				10	52	6			27	1	25	1	12	2	6	2	4	2
Orbulina suturalis Brönnimann													1					
Orbulina universa d'Orbigny				15	16	4			4	1	8		7		8	1	1	
Orbulina bilobata (d'Orbigny)																		
Globorotalia menardii (Parker, Jones & Brady)				6	2				2	5	1		1	1	2		1	1
Globorotalia limbata (Fornasini)									1									
Globorotalia multicamerata Cushman & Jarvis									1									
Globorotalia plesiotumida Blow & Banner																		
Globorotalia tumida (Brady)					3				3		1			1	1		1	
Globorotalia flexuosa (Koch)																		
Globorotalia ungulata Bermúdez																		
Globorotalia scitula (Brady)					1													
Globorotalia conoidea Walters																		
Globoratalia conomiozea Kennett																		
Globorotalia inflata d'Orbigny				34	11	27			21	40	1		2	1	6		8	7
Globorotalia crassaformis (Galloway & Wissler)				1	10	8				1								
Globorotalia crassula Cushman and Stewart																		
Globorotalia tosaensis Takayanagi & Saito																		
Globoquadrina venezuelana (Hedberg)																		
Globoquadrina dehiscens (Chapman, Parr & Collins)																		
Globoquadrina baroemoenensis (LeRoy)																		
Dentoglobigerina altispira altispira (Cushman & Jarvis)									2									
Neogloboquadrina acostaensis (Blow)																		
Neogloboquadrina humerosa (Takayanagi & Saito)				75	17	66			42	9	25	1	8	8	54	3	14	15
Pulleniatina primalis Banner & Blow																		
Pulleniatina obliquiloculata (Parker & Jones)				28	7	2			4	18				4	27	3	4	9
Sphaeroidinellolsis seminulina (Schwager)					1?				2		1						1?	
Sphaeroidinellolsis seminulina (Schwager) (immature form)																		
Sphaeroidinellolsis subdehiscens Blow																		
Sphaeroidinellolsis subdehiscens Blow (immature form)				3	1	1			1		2				2			
Sphaeroidinella dehiscens (Parker & Jones)				34	21	7			7		14	1	6	9	19		7	9
Globigerinita glutinata (Egger)					4				6	1	1						2	
Globigerinella obesa (Bolli)									2									
Globigerinella aequilateralis (Brady)					4													
Globigerinella calida (Parker)																		
Candeina nitida d'Orbigny																		
Total number				221	205	132			189	81	103	4	90	32	270	19	49	49

Table A4
Check-list of calcareous nannofossils identified in the Antung-Chi section.

Study section	Autung-Chi section																					
Sample number	AT01	AT02	AT03	AT04	AT05	AT06	AT07	AT08	AT09	AT10	AT11	AT12	AT13	AT14	AT15	AT16	AT17	AT18	AT19	AT20	AT21	AT22
Stratigraphic unit	TK	TK	TK	TK	TK	TK	TK	TK	TK	TK	TK	TK	TK	LC	LC	LC	LC	LC	LC	TK	TK	TK
Coccolithus miopelagicus Bukry																						
Coccolithus pelagicus (Wallich)	R	R	R		R	R	P	R	P	R	P	R	R		P		R	R		P	P	R
Calcidiscus leptoporus (Murray & Blackman)	R			P		P				R	P			P		R		R	P			
Calcidiscus macintyrei (Bukry & Bramlette)	R		R				R	P		R	R	P	R	R			P	R		P		
Ceratolithus acutus Gartner & Bukry																						
Ceratolithus rugosus Bukry & Bramlette																				P		
Cyclicargolithus floridanus (Roth & Hay)								P														
Discoaster brouweri Tan		P		P		P		P	P	P	F	R	P				P			R	P	
Discoaster pentaradiatus Tan	P																					
Discoaster surculus Martini & Bramlette					P						P							P				
Discoaster variabilis Martini & Bramlette							P				R											
Gephyrocapsa spp. (small)						R												R				R
Gephyrocapsa oceanica Kamptner (medium)																						
Helicosphaera ampliaperta Bramlette & Wilcoxon																						
Helicosphaera carteri (Wallich)	P	P																				
Helicosphaera sellii Bukry & Bramlette				R				P	R						R		R		P			R
Pseudoemiliania lacunosa (Kamptner)	R	F	R		R	R		R		R	F		F	R	R	R	R	R	R		R	R
Reticulofenestra pseudoumbilica (Gartner)	R	F	R	R		R	R	R	R	R	R	R	R	R	R	R	R	R	R	R	R	R
Sphenolithus abies Deflandre	R	R	R	R	R	R		R	R		R	R	R	R	R	R	R	R	P	R		
Sphenolithus heteromorphus Deflandre																						
Sphenolithus moriformis Brönnimann &Stradner			R	R	R	R		R	R					R		R		R		P		R

Study section	Autung-Chi section																			
Sample number	AT23	AT24	AT25	AT26	AT27	AT28	AT29	AT30	AT31	AT32	AT33	AT34	AT35	AT36	AT37	AT38	AT39	AT40	AT41
Stratigraphic unit	TK	TK	TK	TK	TK	TK	TK	LC	TK	TK	TK	TK	TK	TK	TK	TK	TK	TK	TK
Coccolithus miopelagicus Bukry																			
Coccolithus pelagicus (Wallich)		P		P	R	R		P					E	R	R	R	R	P	P
Calcidiscus leptoporus (Murray & Blackman)			P						P			R	R	F	R	R		P	P
Calcidiscus macintyrei (Bukry & Bramlette)	P	R	P	R	R		R		P			R	R	R	R	P	P		
Ceratolithus acutus Gartner & Bukry																			
Ceratolithus rugosus Bukry & Bramlette																			
Cyclicargolithus floridanus (Roth & Hay)																			
Discoaster brouweri Tan	R			R				R						R		R			R
Discoaster pentaradiatus Tan								P											
Discoaster surculus Martini & Bramlette				P				P											
Discoaster variabilis Martini & Bramlette		P												P	P				
Gephyrocapsa spp. (small)		R			R		R		R			R		P	R	R	R	F	
Gephyrocapsa oceanica Kamptner (medium)																			
Helicosphaera ampliaperta Bramlette & Wilcoxon																			
Helicosphaera carteri (Wallich)																			
Helicosphaera sellii Bukry & Bramlette	P		P								P	R		F	R		P	F	
Pseudoemiliania lacunosa (Kamptner)	R	R	R	R	R	R	R	P	R		P	F	F	R	R	R	F	F	R
Reticulofenestra pseudoumbilica (Gartner)	R	F	R	P	R		R		R	P	P	R	R	C	F	R	R	F	F
Sphenolithus abies Deflandre	R	R	R	R	R	R	R	R	R	R		R	R	R	R	R	R	R	R
Sphenolithus heteromorphus Deflandre								P	P										
Sphenolithus moriformis Brönnimann &Stradner			R	R			R		P				R	R			P	P	

Table A5
Check-list of planktonic foraminifera identified in the Wujiang-Chi and the Amei-Chi sections.

Study section	Wujiang-Chi section																
Sample number	WJ01	WJ02	WJ03	WJ04	WJ05	WJ06	WJ07	WJ08	WJ09	WJ10	WJ11	WJ12	WJ13	WJ14	WJ15	WJ16	WJ17
Stratigraphic unit	LC	TK	TK	TK	TK	TK	TK	TK	TK	TK	TK	TK	TK	TK	TK	TK	TK
Globigerina bulloides d'Orbigny																	
Globigerina parabulloides Blow						1											
Globigerina falconensis Blow					4	1			2								
Globigerina woodi Jenkins				1													
Globigerina nepenthes Todd															1?		
Globigerina decoraperta Takayanagi & Saito				5											1		
Globigerina rubescens Hofker			3?		1								1				
Globigerinoides triloba (Reuss)		17	4	14	27	10	2	12	39	13		9	14	14	27	40	40
Globigerinoides immaturus Leroy		25	12	17	22	12	7	7	38	17		5	3	7	17	31	22
Globigerinoides sacculifer (Brady)		32	5	9	9	11	5	9	42	29		21	20	15	13	27	36
Globigerinoides fistulosus (Schubert)					1												
Globigerinoides obliquus Bolli			4		4			1									
Globigerinoides extremus Bolli & Bermúdez		1		4	9	7			2	3		1			1	1	3
Globigerinoides bollii Blow																	
Globigerinoides conglobatus (Brady)		3	2	2	4	3	3	5	10	10		2	10	16	5	11	10
Globigerinoides ruber (d'Orbigny)		38	29	15	61	11	16	25	45	33		24	38	7	25	34	33
Orbulina suturalis Brönnimann			1						1								
Orbulina universa d'Orbigny		8	13	6	6		2	3	32	16		9	23	22	9	20	32
Orbulina bilobata (d'Orbigny)																	
Globorotalia menardii (Parker, Jones & Brady)		20	1	30	21	32	80	62	14	16		54	40	42	74	20	16
Globorotalia limbata (Fornasini)			3	2	15	7	1	9	14	7		1	4	2	5	3	2
Globorotalia multicamerata Cushman & Jarvis		3			2	1			2						2		
Globorotalia plesiotumida Blow & Banner																	
Globorotalia tumida (Brady)		6	4	1	3	7	2	16	8	4		16	11	14	24	9	7
Globorotalia flexuosa (Koch)		3			4			3				6	2		1		
Globorotalia ungulata Bermúdez					2												
Globorotalia scitula (Brady)																	
Globorotalia conoidea Walters																	
Globoratalia conomiozea Kennett																	
Globorotalia inflata d'Orbigny		3				1											
Globorotalia crassaformis (Galloway & Wissler)			1	1		2		3	6	4		1	3		9	5	12
Globorotalia crassula Cushman and Stewart																	
Globorotalia tosaensis Takayanagi & Saito					2												
Globoquadrina venezuelana (Hedberg)																	
Globoquadrina dehiscens (Chapman, Parr & Collins)																	
Globoquadrina baroemoenensis (LeRoy)																	
Dentoglobigerina altispira altispira (Cushman & Jarvis)													1?	1?			
Neogloboquadrina acostaensis (Blow)																	
Neogloboquadrina humerosa (Takayanagi & Saito)		26	13	41	13	15	14	15	25	63		14	17	10	33	36	31
Pulleniatina primalis Banner & Blow					1				1								
Pulleniatina obliquiloculata (Parker & Jones)					1				16					1		5	
Sphaeroidinellolsis seminulina (Schwager)		1?												1			
Sphaeroidinellolsis seminulina (Schwager) (immature form)								1									
Sphaeroidinellolsis subdehiscens Blow										2				2			
Sphaeroidinellolsis subdehiscens Blow (immature form)			3		1			4							4		
Sphaeroidinella dehiscens (Parker & Jones)		8	22	13	20	14	11	37	25	17		73	25	141	55	41	23
Globigerinita glutinata (Egger)			1	21		3	3	1		2		1	4			13	1
Globigerinella obesa (Bolli)					1	1				1							
Globigerinella aequilateralis (Brady)									5	9		1	10		2		
Globigerinella calida (Parker)										1?			1				
Candeina nitida d'Orbigny																	
Total number		194	121	182	234	139	146	213	327	247		238	227	295	308	296	268

Study section	Wujiang-Chi section													
Sample number	WJ18	WJ19	WJ20	WJ21	WJ22	WJ23	WJ24	WJ25	WJ26	WJ27	WJ28	WJ29	WJ30	WJ31
Stratigraphic unit	TK	TK	TK	TK	LC	LC	p. m	p. m	p. m	p. m	p. m	p. m	p. m	p. m
Globigerina bulloides d'Orbigny														
Globigerina parabulloides Blow							1							
Globigerina falconensis Blow														
Globigerina woodi Jenkins														
Globigerina nepenthes Todd	3			5			71	4			20			
Globigerina decoraperta Takayanagi & Saito				4							1			
Globigerina rubescens Hofker									1					
Globigerinoides triloba (Reuss)	22	16	15	35			19	14	38	3	50		3	17
Globigerinoides immaturus Leroy	3	3	6	37			8	5	8		13			2
Globigerinoides sacculifer (Brady)		13	42	20			11	8	4	2	8			4
Globigerinoides fistulosus (Schubert)				1										
Globigerinoides obliquus Bolli		1		7			3	2	1		19			
Globigerinoides extremus Bolli & Bermúdez	1		1	6			19			1?	21			2
Globigerinoides bollii Blow											2			
Globigerinoides conglobatus (Brady)			10	8			2	1			2			
Globigerinoides ruber (d'Orbigny)	9	32	33	42			4		25	2	9		4	15
Orbulina suturalis Brönnimann				2			2		1		1			
Orbulina universa d'Orbigny		2	15	30			29	4	4	1	11			2
Orbulina bilobata (d'Orbigny)														
Globorotalia menardii (Parker, Jones & Brady)		25	10	18				1	4	15				
Globorotalia limbata (Fornasini)	1	7	16	16			25	2		1	7			1
Globorotalia multicamerata Cushman & Jarvis		2	9				1			2				
Globorotalia plesiotumida Blow & Banner	1?										4			
Globorotalia tumida (Brady)	3	2	2	16			1		7	1				
Globorotalia flexuosa (Koch)		1												
Globorotalia ungulata Bermúdez				2?										
Globorotalia scitula (Brady)				1										
Globorotalia conoidea Walters							13							
Globoratalia conomiozea Kennett							6							
Globorotalia inflata d'Orbigny	2			2					17		3			8
Globorotalia crassaformis (Galloway & Wissler)		52	3	9					9	1?	1?			
Globorotalia crassula Cushman and Stewart														
Globorotalia tosaensis Takayanagi & Saito				1										
Globoquadrina venezuelana (Hedberg)				1										
Globoquadrina dehiscens (Chapman, Parr & Collins)											4			
Globoquadrina baroemoenensis (LeRoy)							1				2			
Dentoglobigerina altispira altispira (Cushman & Jarvis)	1						1	3			18			
Neogloboquadrina acostaensis (Blow)													1	
Neogloboquadrina humerosa (Takayanagi & Saito)	3	25	22	64			11	3	46	1	10		2	15
Pulleniatina primalis Banner & Blow							5							
Pulleniatina obliquiloculata (Parker & Jones)				1			1?		2	2				3
Sphaeroidinellolsis seminulina (Schwager)				1			18	6			1			
Sphaeroidinellolsis seminulina (Schwager) (immature form)														1
Sphaeroidinellolsis subdehiscens Blow			1	10			20	9			3			
Sphaeroidinellolsis subdehiscens Blow (immature form)		2	3						1					1
Sphaeroidinella dehiscens (Parker & Jones)	2	26	32	29			1?		17	5	2			13
Globigerinita glutinata (Egger)		2		1					11					
Globigerinella obesa (Bolli)														
Globigerinella aequilateralis (Brady)				2										1
Globigerinella calida (Parker)														
Candeina nitida d'Orbigny														
Total number	52	211	220	371			273	62	196	37	211		10	85

Table A6
Check-list of calcareous nannofossils identified in the Wujiang-Chi and the Amei-Chi sections.

Study section	Wujiang-Chi section															
	WJ01 LC	WJ02 TK	WJ03 TK	WJ04 TK	WJ05 TK	WJ06 TK	WJ07 TK	WJ08 TK	WJ09 TK	WJ10 TK	WJ11 TK	WJ12 TK	WJ13 TK	WJ14 TK	WJ15 TK	WJ16 TK
Coccolithus miopelagicus Bukry																
Coccolithus pelagicus (Wallich)			P	P		R			R		R		R	P	R	
Calcidiscus leptoporus (Murray & Blackman)		R	R		R	R	R		P			R	P	P	P	R
Calcidiscus macintyrei (Bukry & Bramlette)						R		R	P		P	R	R	R	R	R
Ceratolithus acutus Gartner & Bukry																
Ceratolithus rugosus Bukry & Bramlette																
Cyclicargolithus floridanus (Roth & Hay)								P	P							
Cyclicargolithus abisectus (Müller)																
Discoaster asymmetricus Gartner																P
Discoaster brouweri Tan			R	R		P	P	P			P	P	P	P		
Discoaster surculus Martini & Bramlette																R
Discoaster variabilis Martini & Bramlette																
Gephyrocapsa spp. (small)			R		R	R	R	R								
Gephyrocapsa oceanica Kamptner (medium)																
Helicosphaera ampliaperta Bramlette & Wilcoxon																
Helicosphaera carteri (Wallich)					P				P				P			
Helicosphaera perch-nielseniae Haq																
Helicosphaera sellii Bukry & Bramlette			R		R	R		P	R						P	R
Pseudoemiliania lacunosa (Kamptner)		R	F	F	F	F	R	F	C		R	R	R	A	C	R
Reticulofenestra pseudoumbilica (Gartner)			R	R	R	A			F		R	R	R	A	A	F
Sphenolithus abies Deflandre		R	R	R	R	R	P	R	R		R	R	R	R	R	R
Sphenolithus conicus Bukry											P					
Sphenolithus heteromorphus Deflandre																
Sphenolithus moriformis Brönnimann &Stradner				R			P	P			P		P			P

Study section	Wujiang-Chi section															Amei-Chi	
	WJ17 TK	WJ18 TK	WJ19 TK	WJ20 TK	WJ21 TK	WJ22 LC	WJ23 LC	WJ24 p. m	WJ25 p. m	WJ26 p. m	WJ27 p. m	WJ28 p. m	WJ29 p. m	WJ30 p. m	WJ31 p. m	AM01 LC	AM02 LC
Coccolithus miopelagicus Bukry																	
Coccolithus pelagicus (Wallich)	P	P			P	R				R		P	R	R			
Calcidiscus leptoporus (Murray & Blackman)				R	R			R	P					R			R
Calcidiscus macintyrei (Bukry & Bramlette)	R	P	R		R					R			R				
Ceratolithus acutus Gartner & Bukry																	
Ceratolithus rugosus Bukry & Bramlette																	
Cyclicargolithus floridanus (Roth & Hay)																P	
Cyclicargolithus abisectus (Müller)							P										
Discoaster asymmetricus Gartner			P		P												
Discoaster brouweri Tan			R	P	R	P		R									
Discoaster surculus Martini & Bramlette					P			P		P						P	
Discoaster variabilis Martini & Bramlette								R									
Gephyrocapsa spp. (small)		P															F
Gephyrocapsa oceanica Kamptner (medium)																	
Helicosphaera ampliaperta Bramlette & Wilcoxon	P																
Helicosphaera carteri (Wallich)			P														
Helicosphaera perch-nielseniae Haq																	P
Helicosphaera sellii Bukry & Bramlette				P	R			P	P	R			R				R
Pseudoemiliania lacunosa (Kamptner)	R	R	R	R	A			F	P	C							R
Reticulofenestra pseudoumbilica (Gartner)	R	R	F	R	F	R		F		A		R	R	R			F
Sphenolithus abies Deflandre	R	R	P	R	R	R		R	P	R		R	R	R		R	F
Sphenolithus conicus Bukry																	
Sphenolithus heteromorphus Deflandre						P											
Sphenolithus moriformis Brönnimann &Stradner								R				R		R			C

Table A7
Check-list of planktonic foraminifera identified in the Loho forearc basin by Chang (1969).

Study section	Loho-Chi section																				
Sample number	C16	C17	A44	A45	A46	A47	A48	A49	A50	A51	A52	A56	A57	A58	A59	A60	A61	A62	A65	A66	A67	A68
Stratigraphic unit	LC	LC	TK	TK	TK	TK	TK	TK	TK	TK	TK	TK	TK	TK	TK	TK	TK	TK	TK	TK	TK	TK
Globigerina bulloides d'Orbigny																						
Globigerina parabulloides Blow																						
Globigerina falconensis Blow																						
Globigerina woodi Jenkins																						
Globigerina nepenthes Todd					?										D		?				D	
Globigerina decoraperta Takayanagi & Saito																						
Globigerina rubescens Hofker																						
Globigerinoides triloba (Reuss)			V	V	V		R	A	R	C	R	V	V	V	V	C	A				R	R
Globigerinoides immaturus Leroy			C		C	C	A	F	C	A		F	R	F								
Globigerinoides sacculifer (Brady)			A	A	A	R	F	F		R		C	A	C	R	R					R	
Globigerinoides fistulosus (Schubert)			R		R									R								
Globigerinoides obliquus Bolli			D		D					D					D		?					
Globigerinoides extremus Bolli & Bermúdez										D												
Globigerinoides bollii Blow																						
Globigerinoides conglobatus (Brady)			A			R	C															
Globigerinoides ruber (d'Orbigny)			V	A	A	R	?	R	?			F	C	F	R	R	F					
Globigerinoides. spp.			F	R	R		R	R	A				R	R								
Orbulina suturalis Brönnimann			R	R	R			R				R		R		R						
Orbulina universa d'Orbigny			V	V	V	F	C	A	F	C	?	V	V	V	C	A	R		R		C	R
Orbulina bilobata (d'Orbigny)			R		R							R										
Globorotalia menardii (Parker, Jones & Brady)			F	F	A	F	C	C	R	A		V	A	A	C	F	R	R			C	R
Globorotalia limbata (Fornasini)																						
Globorotalia miocenica Palmer			D																			
Globorotalia multicamerata Cushman & Jarvis			C	?	R			R		R		R		R								
Globorotalia plesiotumida Blow & Banner																						
Globorotalia tumida (Brady)			V	A	A	R	F	F	R	F		A	F	C	A	R	R	R			R	R
Globorotalia flexuosa (Koch)																						
Globorotalia ungulata Bermúdez																						
Globorotalia scitula (Brady)			R									R										
Globorotalia conoidea Walters																						
Globoratalia conomiozea Kennett																						
Globorotalia inflata d'Orbigny																						
Globorotalia crassaformis (Galloway & Wissler)			A	C	C	R	A	R	C	?		C	A	F	F	C	F					
Globorotalia crassula Cushman & Stewart																						
Globorotalia tosaensis Takayanagi & Saito						R			?			R	R		R		R					
Globorotalia spp.							R	R							R							
Globoquadrina venezuelana (Hedberg)			D							D		D			D		D					
Globoquadrina dehiscens (Chapman, Parr & Collins)																						
Globoquadrina baroemoenensis (LeRoy)																						
Globoquadrina sp.			D																		D	
Dentoglobigerina altispira altispira (Cushman & Jarvis)			D							D		D			D							
Neogloboquadrina acostaensis (Blow)								?	R			R			F							
Neogloboquadrina humerosa (Takayanagi & Saito)			C	A	V			R	F			R	A	F		F						R
Neogloboquadrina dutertrei (d'Orbigny)			C			F			R				F			C	R					
Pulleniatina primalis Banner & Blow				R										?		R						
Pulleniatina obliquiloculata (Parker & Jones)			R	R	F	R			R	R					R	C						
Sphaeroidinellolsis seminulina (Schwager)			D							D					D						D	
Sphaeroidinellolsis kochi Caudri																					D	
Sphaeroidinellolsis subdehiscens Blow			F	R		?				?	R											
Sphaeroidinellolsis subdehiscens Blow (immature form)																						
Sphaeroidinella dehiscens (Parker & Jones)	√	√	V	V	A	A	V	A	A	C		V	V	V	A	C	C	?	R	R	R	R
Globigerinita glutinata (Egger)			?	?									R		R		?					

Globigerinella obesa (Bolli)																				
Globigerinella aequilateralis (Brady)			?	R	R		R													
Globigerinella calida (Parker)																				
Candeina nitida d'Orbigny			F	A	A	R		R		R		A	A	F	R	F			R	
Study section	Antung-Chi section									Amei-Chi section										
Sample number	A96	A97	A99	A100	A102	A103	A105	A106	A107	A111	A112	A113	A114	A116	A117	A118	A119	A120	A121	
Stratigraphic unit	LC	LC	TK	TK	TK	TK	TK	TK	TK	LC	LC	LC	LC	TK	TK	TK	TK	TK	TK	
Globigerina bulloides d'Orbigny											R				R					
Globigerina parabulloides Blow																				
Globigerina falconensis Blow																				
Globigerina woodi Jenkins																				
Globigerina nepenthes Todd																				
Globigerina decoraperta Takayanagi & Saito																				
Globigerina rubescens Hofker																				
Globigerinoides triloba (Reuss)	R	F	A	R	R	C	F	R		A	R	C	A	C	C		V	R	V	
Globigerinoides immaturus Leroy																				
Globigerinoides sacculifer (Brady)		R	F			R	R			C		R	R	R	F		C		A	
Globigerinoides fistulosus (Schubert)																				
Globigerinoides obliquus Bolli			D							D		?								
Globigerinoides extremus Bolli & Bermúdez										D										
Globigerinoides bollii Blow																				
Globigerinoides conglobatus (Brady)			R							F							R			
Globigerinoides ruber (d'Orbigny)		R				C					R		R		F		R		R	
Globigerinoides. spp.																?				
Orbulina suturalis Brönnimann																	R			
Orbulina universa d'Orbigny		C	A			C	C			V	R	V	A	R	C		C		A	
Orbulina bilobata (d'Orbigny)										R										
Globorotalia menardii (Parker, Jones & Brady)	F	C	C			R	C		R	C		V	R		F		C	R	C	
Globorotalia limbata (Fornasini)																				
Globorotalia miocenica Palmer																				
Globorotalia multicamerata Cushman & Jarvis																				
Globorotalia plesiotumida Blow & Banner																				
Globorotalia tumida (Brady)	F	R	F			R	C			C		V	F	R	R		F		F	
Globorotalia flexuosa (Koch)																				
Globorotalia ungulata Bermúdez																				
Globorotalia scitula (Brady)																				
Globorotalia conoidea Walters																				
Globoratalia conomiozea Kennett																				
Globorotalia inflata d'Orbigny																				
Globorotalia crassaformis (Galloway & Wissler)		R	R			A		C	C	F			A	R	A		C	R	V	
Globorotalia crassula Cushman & Stewart																				
Globorotalia tosaensis Takayanagi & Saito			?												R					
Globorotalia spp.																				
Globoquadrina venezuelana (Hedberg)										D										
Globoquadrina dehiscens (Chapman, Parr & Collins)																				
Globoquadrina baroemoenensis (LeRoy)																				
Globoquadrina sp.																				
Dentoglobigerina altispira altispira (Cushman & Jarvis)			D							D										
Neogloboquadrina acostaensis (Blow)																		?		
Neogloboquadrina humerosa (Takayanagi & Saito)															C		R		A	
Neogloboquadrina dutertrei (d'Orbigny)		F			R	?	?	?	?				C	F			R			
Pulleniatina primalis Banner & Blow																		R		
Pulleniatina obliquiloculata (Parker & Jones)		R			R	?	?			C			R		C		R			
Sphaeroidinellolsis seminulina (Schwager)			D	D						D		D								
Sphaeroidinellolsis kochi Caudri			D							D										
Sphaeroidinellolsis subdehiscens Blow			D						R											
Sphaeroidinellolsis subdehiscens Blow (immature form)																				
Sphaeroidinella dehiscens (Parker & Jones)	A	V	R		R	A	A	A	C	C		A	V	C	C	R	V	R	V	

Table A7 (*continued*)

Study section	Antung-Chi section									Amei-Chi section									
Sample number	A96	A97	A99	A100	A102	A103	A105	A106	A107	A111	A112	A113	A114	A116	A117	A118	A119	A120	A121
Stratigraphic unit	LC	LC	TK	TK	TK	TK	TK	TK	TK	LC	LC	LC	LC	TK	TK	TK	TK	TK	TK
Globigerinita glutinata (Egger)																			
Globigerinella obesa (Bolli)																			
Globigerinella aequilateralis (Brady)																			
Globigerinella calida (Parker)																			
Candeina nitida d'Orbigny		R	R				R		R	C		A	F		R		F		R

Notes: $R<6$, $F=6$–10, $C=11$–20, $A=21$–50, $V>50$, ?=Identified, D=reworked, $\surd$=present without detailed abundance.
Some of the species' name in Chang (1969) have been revised as followed: *G. (T.)* spp.=*Globorotalia* spp. (in this table). *Neogloboquadrina dutertrei forma subcretacea*=*N. humerosa* (in this table). *Neogloboquadrina dutertrei forma humerosa*=*N. humerosa* (in this table). *Hastigerina siphonifera*=*Globigerinella aequilateralis* (in this table).

Appendix B

Check-list of microfossils identified in the Taitung remnant forearc basin (this study). Including 6 Tables B1–B6.

Table B1
Check-list of planktonic foraminifera identified in the Chili-Chi section.

Study section	Chili-Chi section													
Sample number Lithology	Q01a si.	Q01b si.	Q01c si.	Q01d m.	Q02 m.	Q03 m.	Q04 m.	Q05 m.	Q06 m.	Q07 m.	Q08 m.	Q09 m.	Q10 m.	Q11 m.
Globigerina parabulloides Blow				1	2					1				
Globigerina bulloides d'Orbigny														
Globigerina falconensis Blow	2		1	1	4								1	
Globigerina woodi Jenkins						1								
Globigerina decoraperta Takayanagi & Saito											2			
Globigerina rubescens Hofker														1
Globigerinoides triloba (Reuss)	15	29	21	25	6	2	1			1	15	4	4	
Globigerinoides immaturus Leroy	21	12	37	24	7		1	1		2	4	1	1	
Globigerinoides sacculifer (Brady)	36	48	51	39	6	1				4	11	8	9	4
Globigerinoides fistulosus (Schubert)	7	1												
Globigerinoides obliquus Bolli										1				
Globigerinoides extremus Bolli & Bermúdez	10				1							2		
Globigerinoides conglobatus (Brady)	2	9	12	7	2	1							3	
Globigerinoides ruber (d'Orbigny)	32	37	44	38	30	4			1	16	33	8	6	2
Orbulina suturalis Brönnimann			1											
Orbulina universa d'Orbigny	9	6	18	8	2					16	1			
Globorotalia menardii (Parker, Jones & Brady)	6	13	37	21	11	9	5			11	5	2	12	
Globorotalia limbata (Fornasini)	7	7	11	4										
Globorotalia multicamerata Cushman & Jarvis	9	3		4										
Globorotalia tumida (Brady)	3	6	13	8	9				1	3	9	11	12	3
Globorotalia flexuosa(Koch)		3			1								1	
Globorotalia ungulata Bermúdez			1											
Globorotalia scitula (Brady)		1									1			
Globorotalia inflata d'Orbigny					14	3	1			33	35	16	83	4
Globorotalia puncticulata (Deshayes)	?1													
Globorotalia crassaformis (Galloway & Wissler)	10	9	7	6									1	
Globorotalia tosaensis Takayanagi & Saito	1			12	8						1		7	
Globorotalia truncatulinoides d'Orbigny					?1								1	
Globorotalia sp.			1								1	1		
Dentoglobigerina altispira altispira (Cushman & Jarvis)														
Neogloboquadrina pachyderma (Ehrenberg)											1			
Neogloboquadrina humerosa (Takayanagi & Saito)	23	14	37	10	70	27	1			51	61	31	31	5
Pulleniatina primalis Banner & Blow														
Pulleniatina obliquiloculata (Parker & Jones)	1	8	8	9	55	2	1			38	18	2	18	
Sphaeroidinellolsis subdehiscens Blow (immature form)					2						3			
Sphaeroidinella dehiscens (Parker & Jones)	10	6	24	8	16	2	2	1		16	11	15	12	15
Globigerinita glutinata (Egger)	1										10			
Globigerinella obesa (Bolli)	1													
Globigerinella aequilateralis (Brady)	3		4	5	3									
Candeina nitida d'Orbigny					?1									
Total number	210	212	328	230	251	52	12	2	2	193	222	101	202	34

Notes: Lithology of Takangkou Formation, sa — sandstone; si. — siltstone; m. — mudstone; p.m. — pebbly mudstone.

Table B2
Check-list of calcareous nannofossils identified in the Chili-Chi section.

Study section	Chili-Chi section													
Sample number Lithology	Q01a si.	Q01b si.	Q01c si.	Q01d m.	Q02 m.	Q03 m.	Q04 m.	Q05 m.	Q06 m.	Q07 m.	Q08 m.	Q09 m.	Q10 m.	Q11 m.
Calcidiscus leptoporus (Murray & Blackman)	F	F	R	F						R	F	R	R	R
Calcidiscus macintyrei (Bukry & Bramlette)	R	R		F						R		R		P
Ceratolithus cristatus Kamptner														
Ceratolithus rugosus Bukry & Bramlette														
Coccolithus sp. (small)	A	A		F										
Coccolithus pelagicus (Wallich)														
Crenalithus doronicoides (Black & Barnes)	A	A	F	C		C	C	C	F	C		F	C	
Cyclicargolithus floridanus (Roth & Hay)	P													
Discoaster sp.	F	R		R	R				R					
Discoaster cf. *exilis* Martini & Worsley														
Discoaster pentaradiatus Tan														
Discoaster quinqueramus Gartner														
Discoaster surculus Martini & Bramlette														
Discoaster variabilis Martini & Bramlette														
Discolithina sp.	P													
Gephyrocapsa spp. (small)														
Gephyrocapsa cf. *oceanica* Kamptner (medium)														
Gephyrocapsa oceanica Kamptner (large)														
Helicosphaera kamptneri Hay & Mohler	F	F	R	R		R	P	R	R	R		F	R	R
Helicosphaera sellii Bukry & Bramlette	R	R	R	R					R	R			R	R
Pseudoemiliania lacunosa (Kamptner)	C	C	R	A	R	C	F	C	F	C	A	C	C	
Pseudoemiliania ovata (Bukry) synonym														
Reticulofenestra minuta Roth														
Reticulofenestra pseudoumbilica (Gartner) (small)	R	R		F		R	R	R	R	R	R			R
Reticulofenestra pseudoumbilica (Gartner) (medium)	R	P	P			C	F	F	F	C	A		C	
Reticulofenestra pseudoumbilica (Gartner) (large)														
Rhabdosphaera clavigera Murray & Blackman														
Sphenolithus sp.		P		P	P		P		P		P	P		P
Sphenolithus abies Deflandre														
Sphenolithus moriformis Brönnimann &Stradner														
Syracosphaera sp.	P	R												

Notes for abundance: A=abundant; C=common; F=few; R=rare; P=present.

Table B3
Check-list of planktonic foraminifera identified in the Tengchiao-Chi section.

Study section	Tengchiao-Chi section												Hsinchiao	
Sample number Lithology	T02 m.	T03 m.	T04 m.	T05 m.	T07 m.	T08 m.	T09 m.	T10 m.	T11 m.	T12 m.	T13 m.	T14 m.	X02 m.	X01 m.
Globigerina parabulloides Blow														
Globigerina bulloides d'Orbigny	1					1	6	4	12	6	9	7	4	5
Globigerina falconensis Blow														
Globigerina woodi Jenkins														
Globigerina decoraperta Takayanagi & Saito														
Globigerina rubescens Hofker							3	1	7	3				
Globigerinoides triloba (Reuss)	3	20	2	4		17	6	8	11	6	14	22	20	30
Globigerinoides immaturus Leroy	2	21		1		8			4	11	15	22	14	9
Globigerinoides sacculifer (Brady)	3	12	1	4		16	8	1	4	11	9	14	4	2
Globigerinoides fistulosus (Schubert)														
Globigerinoides obliquus Bolli		1												
Globigerinoides extremus Bolli & Bermúdez														
Globigerinoides conglobatus (Brady)		4		3		3			1	4			2	3
Globigerinoides ruber (d'Orbigny)	4	11	2	5		10	28	63	51	51	36	45	75	72
Orbulina suturalis Brönnimann														
Orbulina universa d'Orbigny		6		2		5	4			2		2	1	
Globorotalia menardii (Parker, Jones & Brady)	2	10	6	10	1	1	8	2	3	7	4			
Globorotalia limbata (Fornasini)		9												
Globorotalia multicamerata Cushman & Jarvis														
Globorotalia tumida (Brady)	1	14	4	4		2	3	3	9	2	1	24	20	9
Globorotalia flexuosa(Koch)								1		2				
Globorotalia ungulata Bermúdez										1				
Globorotalia scitula (Brady)								1	2	2	1		1	2
Globorotalia inflata d'Orbigny	5	7		23	1	15	13	19	7		2	12	69	27
Globorotalia puncticulata (Deshayes)														
Globorotalia crassaformis (Galloway & Wissler)		1	1			8	1	2					5	
Globorotalia tosaensis Takayanagi & Saito		5				1		5	4		14	34	9	1
Globorotalia truncatulinoides d'Orbigny							1				1		3	1
Globorotalia sp.								1						1
Dentoglobigerina altispira altispira (Cushman & Jarvis)		1												
Neogloboquadrina pachyderma (Ehrenberg)	1	1												
Neogloboquadrina humerosa (Takayanagi & Saito)	16	24	24	99		90	89	38	28	65	118	54	46	69
Pulleniatina primalis Banner & Blow														
Pulleniatina obliquiloculata (Parker & Jones)	15	7	7	5		44	51	4	10	26	27	27	20	20
Sphaeroidinellolsis subdehiscens Blow (immature form)		1												
Sphaeroidinella dehiscens (Parker & Jones)	8	58	9	6		2	9	17	5	3	3	12	11	15
Globigerinita glutinata (Egger)				1			2	24	41	10	11	18	13	19
Globigerinella obesa (Bolli)											?1			
Globigerinella aequilateralis (Brady)				1										
Candeina nitida d'Orbigny														
Total number	61	213	56	168	2	223	232	194	199	212	266	293	317	285

Table B4
Check-list of calcareous nannofossils identified in the Tengchiao-Chi section.

Study section	Tengchiao-Chi section														Hsinchiao	
Sample number	T02	T03	T04	T05	T05	T07	T08	T09	T10	T11	T12	T13	T14	T15	X02	X01
Lithology	m.	m.	m.	m.	m.	m.	m.	m.	m.	m.	m.	m.	m.	m.	m.	m.
Calcidiscus leptoporus (Murray & Blackman)	R	R	R	R	R	R	R	R	R	R	R	R	R		F	R
Calcidiscus macintyrei (Bukry & Bramlette)	R	R	R		P	R		P			P				?	R
Ceratolithus cristatus Kamptner	R									P						
Ceratolithus rugosus Bukry & Bramlette			P													
Coccolithus sp. (small)	C		F	F	F	C	C	F	C	F	F					
Coccolithus pelagicus (Wallich)	R	R			P							R				
Crenalithus doronicoides (Black & Barnes)	C	F	C	F	F	C	C	F	F	F	F	F	F		F	C
Cyclicargolithus floridanus (Roth & Hay)	P									R						R
Discoaster cf. *exilis* Martini & Worsley				P												
Discoaster pentaradiatus Tan				R		P	P									
Discoaster quinqueramus Gartner				P							P					
Discoaster surculus Martini & Bramlette																
Discoaster variabilis Martini & Bramlette	P															
Discolithina sp.		P		P		R	R	P	R						R	P
Gephyrocapsa spp. (small)			R	F	R	C	C	F	C	F	F	C	C	R	C	A
Gephyrocapsa cf. *oceanica* Kamptner (medium)				R?		R	R	R	C	F	F	F	F			P
Gephyrocapsa oceanica Kamptner (large)						?	R	R	A	F	F	F	F		C	
Helicosphaera kamptneri Hay & Mohler	R	R		P	P	R	R	R	R	R	R	R	R		F	R
Helicosphaera sellii Bukry & Bramlette	R				P	R	R	R	R						R	R
Pseudoemiliania lacunosa (Kamptner)	C	F	C	F	F	A	C	F	C	F	F	F	F	R	A	C
Pseudoemiliania ovata (Bukry) synonym	R	R	R	F	R	F	R	R	F	R	R	R	R		C	F
Reticulofenestra minuta Roth	F	F		R	R	F	F	R	F	F	F					
Reticulofenestra pseudoumbilica (Gartner) (small)			R	R	R	?	R		R	R		R	R			
Reticulofenestra pseudoumbilica (Gartner) (medium)	R			R		R	F			R						
Reticulofenestra pseudoumbilica (Gartner) (large)		P														
Rhabdosphaera clavigera Murray & Blackman						P										
Shenolithus sp.																
Sphenolithus abies Deflandre	R			P	R	P		P			R					
Sphenolithus moriformis Brönnimann &Stradner	P												P			
Syracosphaera sp.	P			P		P	P									

Table B5
Check-list of planktonic foraminifera identified in the Chunchieh-Chi section.

Study section	Chunchieh-Chi section																Ruchiang-Chi	
Sample number	J01a	J01b	J02	J03	J04	J05	J06a	J06b	J07	J08	J09a	J09b	J10	J12	J13	J14	J15	R06	R07
Lithology	m.	sa.	m.	m.	m.	m.	m.	m.	p.m.	p.m.	p.m.	p.m.	m.	p.m.	p.m.	p.m.	p.m.	m.	m.
Globigerina parabulloides Blow																			
Globigerina bulloides d'Orbigny		1	2						1	1	2								
Globigerina falconensis Blow	3			5	3	4				4				2					
Globigerina woodi Jenkins												2		1					
Globigerina nepenthes Todd									6	14						1	11		
Globigerina decoraperta Takayanagi & Saito	2			1			1			4				1			1	4	
Globigerina rubescens Hofker	10		1	1	2	3			2	1	5		1		1	9	3		
Globigerinoides triloba (Reuss)	9	15	5	1	8	14		13	23	35	6	38	1	5	6	12	47	23	30
Globigerinoides immaturus Leroy		11	1		3	3		6	19	22		39		6	3	3	29		4
Globigerinoides sacculifer (Brady)	1	19	5	2	2	2		16	25	21	3	20		2	1	7	12	1	31
Globigerinoides fistulosus (Schubert)		3										1							
Globigerinoides bollii Blow										5							2	1	
Globigerinoides obliquus Bolli									2	34	2			2			12		
Globigerinoides extremus Bolli & Bermúdez		1							6	17	1	10				1	7		
Globigerinoides conglobatus (Brady)		3			1	1		2	8	7		12				1	3		1
Globigerinoides bulloideus Crescenti																	1		
Globigerinoides ruber d'Orbigny	51	16	16	8	33	27	1	10	50	46	27	32	8	23	10	23	84	35	28
Orbulina suturalis Brönnimann																			
Orbulina universa d'Orbigny		16	1					5	32	6		20	1				5	3	7
Obulina bilobata (d'Orbigny)												1							
Globorotalia menardii (Parker, Jones & Brady)	2	22	24	3	18	4		47	15	6	1	6		1		5	3	5	17
Globorotalia limbata (Fornasini)		3							7	20		11					5	3	5
Globorotalia multicamerata Cushman & Jarvis									1	3		1					1		
Globorotalia plesiotumida Blow & Banner									2	11		2		1			9		
Globorotalia tumida (Brady)	1	6	7		9	8		10	14	6	6	5		9	5	4	19		6
Globorotalia flexuosa (Koch)								1		4									
Globorotalia ungulata Bermúdez		1							5							2			
Globorotalia scitula (Brady)					1			1	3	7		4				1	2	1	
Globorotalia margaritae (Bolli & Bermúdez)									1	3									
Globorotalia conoidea Walters									1	?3									
Globorotalia inflata d'Orbigny		1	1		60	43	2	15	48	7		5				2	20	2	9
Globorotalia puncticulata (Deshayes)																			
Globorotalia crassaformis (Galloway & Wissler)	1	2						2	6	9	1						2		
Globorotalia tosaensis Takayanagi & Saito	1	4	2	2	6	14		3	12	8		4	3				13		
Globorotalia truncatulinoides d'Orbigny	1			2	2	2		3	23	1	1	1	4	1			1	?1	
Globorotalia humilis (Brady)					?1														
Globorotalia sp.										2					1	3			
Globoquadrina dehiscens (Chapman, Parr & Collins)										2									
Dentoglobigerina altispira altispira (Cushman & Jarvis)									2	25		8					4		
Neogloboquadrina pachyderma (Ehrenberg)																			
Neogloboquadrina acostaensis (Blow)									2			1							
Neogloboquadrina humerosa (Takayanagi & Saito)	40	40	190	23	108	86	2	104	72	23	28	57	28	41	22	22	78	30	58
Pulleniatina primalis Banner & Blow										1		1							
Pulleniatina obliquiloculata (Parker & Jones)	2	33	37	3	59	11		62	49	8	2	23		3	3	4	16	20	19
Sphaeroidinellolsis seminulina (Schwager)									9	10		6					5		
Sphaeroidinellolsis kochi Caudri									1	3		1							
Sphaeroidinellolsis subdehiscens Blow									2	7	3	1					1		
Sphaeroidinellolsis subdehiscens Blow (immature form)			7	1	4	7								1	1		3	3	5
Sphaeroidinella dehiscens (Parker & Jones)		26	16	4	22	58		40	19	3	8	25	4	26	3	5	30	17	38
Globigerinita glutinata (Egger)	76		10	7	7	29	1	1	7	6	6	4	8	16		10	21	7	
Globigerinella obesa (Bolli)		1								?1		3							
Globigerinella aequilateralis (Brady)		7							5	9		2		1					
Globigerinella calida (Parker)									6	4									
Candeina nitida d'Orbigny	1																		
Total number	201	231	325	63	349	316	7	341	486	409	102	346	58	142	56	115	450	156	258

Table B6
Check-list of calcareous nannofossils identified in the Chunchieh-Chi section.

Study section	Chunchieh-Chi section					
Sample number	J04	J05	J06b	J07	J09b	J10
Calcidiscus leptoporus (Murray & Blackman)	R	R	R	R	R	R
Calcidiscus macintyrei (Bukry & Bramlette)	R	P?	R	R	P	
Ceratolithus cristatus Kamptner						
Ceratolithus rugosus Bukry & Bramlette						
Coccolithus sp. (small)	C	F		C		C
Coccolithus pelagicus (Wallich)		R		F		P
Crenalithus doronicoides (Black & Barnes)	C	C		C		C
Cyclicargolithus abisectus (Müller) (fragment)		P				
Cyclicargolithus floridanus (Roth & Hay)				R		P
Cyclicargolithus cf. *floridanus* (Roth & Hay)	R			R		
Dictyococcites hesslandii (Haq)	R	R		R		P
Discoaster cf. *exilis* Martini & Worsley		P				
Discoaster pentaradiatus Tan						
Discoaster quinqueramus Gartner				R		
Discoaster surculus Martini & Bramlette						
Discoaster variabilis Martini & Bramlette		P				P
Discolithina sp.		R		R		R
Gephyrocapsa spp. (small)	F	F		F		R
Gephyrocapsa cf. *oceanica* Kamptner (medium)	R	R		R		R
Gephyrocapsa oceanica Kamptner (medium)		R		R		R
Helicosphaera kampteri Hay & Mohler	R	R	R	R		R
Helicosphaera sellii Bukry & Bramlette		R	R	R		
Pseudoemiliania lacunosa (Kamptner)	C	F	C	C	F	C
Reticulofenestra minuta Roth	F	R		F		C
Reticulofenestra pseudoumbilica (Gartner) (small)		R	R	F		
Reticulofenestra pseudoumbilica (Gartner) (medium)		R	C	F	R	
Reticulofenestra pseudoumbilica (Gartner) (large)		R		R		R
Rhabdosphaera clavigera Murray & Blackman		P				
Sphenolithus sp.			P			P
Sphenolithus abies Deflandre		R		P		
Sphenolithus abies Deflandre (overgrows)		P		R		
Sphenolithus cf. *belemnos* Bramlette & Wilcoxon		P				
Sphenolithus cf. *heteromorphus* Deflandre				P		
Sphenolithus moriformis Brönnimann & Stradner		P		P		P
Syracosphaera sp.	P	P		R		P

References

Anthonissen, D.E., Ogg, J.G., 2012. Appendix 3—Cenozoic and Cretaceous biochronology of planktonic foraminifera and calcareous nannofossils. In: Gradstein, F.M., Ogg, G.M., Schmitz, M.D., Ogg, G.M. (Eds.), The Geologic Time Scale 2012. Elsevier, Boston, pp. 1083–1127.

Bloomer, S.H., Taylor, B., MacLeod, C.J., Stern, R.J., Fryer, P., Hawkins, J.W., Johnson, L., 1995. Early arc volcanism and the ophiolite problem: a perspective from drilling in the Western Pacific. In: Taylor, B., Natland, J. (Eds.), Active Margins and Marginal Basins of the Western Pacific. AGU Geophysical Monograph Series 88, Washington, DC, pp. 1–30.

Blow, W.H., 1969. Late middle eocene to recent planktonic foraminiferal biostratigraphy. In: Brönnimann, P., Renz, H.H. (Eds.), Proceedings of the First International Conference on Planktonic Microfossils 1. E.J. Brill, Leiden, pp. 199–422.

Bown, P.R., Young, J.R., 1998. Techniques. In: Bown, P.R. (Ed.), Calcareous Nannofossil Biostratigraphy. Kulwer Academic Publications, Dordrecht, Netherlands, pp. 16–28.

Broecker, W.S., 1982. Ocean chemistry during glacial time. Geochim. Cosmochim. Acta 46, 1689–1705.

Chang, C.P., Angelier, J., Huang, C.Y., Liu, C.S., 2001. Structural evolution and significance of a mélange in a collision belt: the Lichi Mélange and the Taiwan arc–continent collision. Geol. Mag. 138, 633–651.

Chang, L.S., 1967. A biostratigraphic study of the Tertiary in the Coastal Range, eastern Taiwan, based on smaller foraminifera (I: Southern Part). Proc. Geol. Soc. China 10, 64–76.

Chang, L.S., 1969. A biostratigraphic study of the Tertiary in the Coastal Range, eastern Taiwan, based on smaller foraminifera (III: Middle Part). Proc. Geol. Soc. China 12, 89–101.

Chen, C.T.A., Huang, M.H., 1996. A mid-depth front separating the South China Sea water and the Philippine Sea water. J. Oceanogr. 52 (1), 17–25.

Chen, W.H., Huang, C.Y., Yan, Y., Chen, D.F., unpublished results. Spatial and temporal variations across a west-east transect of the Lichi Mélange–remnant forearc sequences in the southern Coastal Range: recording tectonics and sedimentation in the forearc basin during active Taiwan arc–continent collision.

Cheng, Y.M., Huang, C.Y., 1975. Biostratigraphic study in the West Hengchun Hill. Acta Geol. Taiwan 18, 49–59.

Chi, W.R., Namson, J., Suppe, J., 1981. Stratigraphic record of plate interactions in the Coastal Range of eastern Taiwan. Mem. Geol. Soc. China 4, 155–194.

Chou, W.C., Sheu, D.D., Chen, C.T., Wen, L.S., Yang, Y., Wei, C.L., 2007. Transport of the South China Sea subsurface water outflow and its influence on carbon chemistry of Kuroshio waters off southeastern Taiwan. J. Geophys. Res. 112, C12008. http://dx.doi.org/10.1029/2007JC004087.

Crowley, T.J., Burke, K.C., 1998. Tectonic Boundary Conditions for Climate Reconstructions. Oxford University Press, New York 285 pp.

Gartner, S., 1990. Neogene calcareous nannofossil biostratigraphy, Leg 116 (Central Indian Ocean). Proceedings of ODP—Scientific Results vol. 116, 165–187.

Hall, R., 2002. Cenozoic geological and plate tectonic evolution of SE Asia and the SW Pacific: computer-based reconstructions, model and animations. J. Asian Earth Sci. 20 (4), 353–431.

Haug, G.H., Tiedemann, R., 1998. Effect of the formation of the Isthmus of Panama on Atlantic Ocean thermohaline circulation. Nature 393 (6686), 673–676. http://dx.doi.org/10.1038/31447.

Horng, C.S., Shea, K.S., 1996. Dating of the Plio-Pleistocene rapidly deposited sequence based on integrated magneto-biostratigraphy: a case study of the Madagida-chi section, Coastal Range, eastern Taiwan. J. Geol. Soc. China 39, 31–58.

Hsu, T.L., 1956. Geology of the Coastal Range, eastern Taiwan. Bull. Geol. Surv. Taiwan 8, 39–64.

Huang, C.Y., Shyu, C.T., Lin, S.B., Lee, T.Q., Sheu, D.D., 1992. Marine geology in the arc–continent collision zone off southeastern Taiwan: implications for late Neogene evolution of the Coastal Range. Mar. Geol. 107, 183–212.

Huang, C.Y., Yuan, P.B., Song, S.R., Lin, C.W., Wang, C., Chen, M.T., Shyu, C.T., Karp, B., 1995. Tectonics of short-lived intra-arc basins in the arc–continent collision terrane of the Coastal Range, eastern Taiwan. Tectonics 14 (1), 19–38.

Huang, C.Y., Wu, W.Y., Chang, C.P., Tsao, S., Yuan, P.B., Lin, C.W., Xia, K.Y., 1997. Tectonic evolution of accretionary prism in the arc–continent collision terrane of Taiwan. Tectonophysics 281, 31–51.

Huang, C.Y., Yuan, P.B., Lin, C.W., Wang, T.K., Chang, C.P., 2000. Geodynamic processes of Taiwan arc–continent collision and comparison with analogs in Timor, Papua New Guinea, Urals and Corsica. Tectonophysics 325, 1–21.

Huang, C.Y., Yuan, P.B., Tsao, S.J., 2006. Temporal and spatial records of active arc–continent in Taiwan: a synthesis. Geol. Soc. Am. Bull. 118, 274–288. http://dx.doi.org/10.1130/B25527.1.

Huang, C.Y., Chien, C.W., Yao, B., Chang, C.P., 2008. The Lichi Mélange: a collision mélange formation along early arcward backthrusts during forearc basin closure, Taiwan arc–continent collision. In: Draut, A.E., Clift, P.D., Scholl D.W. (Eds.), Formation and Applications of Sedimentary Record in Arc Collision Zones. Geol. Soc. Am. Spec. Pap., vol. 436, pp. 127–154. doi: 10.1130/2008.2436 (06).

Huang, C.Y., Yan, Y., Zhao, Q.H., Lin, C.T., 2012. Cenozoic stratigraphy of Taiwan: window into rifting, stratigraphy and paleoceanography of South China Sea. Chin. Sci. Bull. 57, 3130–3149. http://dx.doi.org/10.1007/s11434-012-5349-y.

Huang, C.Y., Lin, Y.J., Lin, C.T., Hsieh, Y.H., Chen W.H., Liu, C.S., Harris, R., Yan, Y., Liu, Z.F., Sun, W.D., unpublished results. Temporal–spatial variations of dynamic forearc sedimentation and development of modern-forming forearc collisional mélange in response to backthrusting during active arc–continent collision, eastern Taiwan.

Huang, T.C., Chen, M.P., Chi, W.R., 1979. Calcareous nannofossils from the red shale of the ophiolite-mélange complex, eastern Taiwan. Mem. Geol. Soc. China 3, 131–138.

Jian, Z., Zhao, Q., Cheng, X., Wang, J., Wang, P., Su, X., 2003. Pliocene–Pleistocene stable isotope and paleoceanographic changes in the northern South China Sea. Palaeogeogr. Palaeoclimatol. Palaeoecol. 193 (3), 425–442. http://dx.doi.org/10.1016/S0031-0182(03)00259-1.

Kao, H., Huang, G.C., 2000. Transition from oblique subduction to collision in the northern Luzon arc–Taiwan region: constraints from bathymetry and seismic observations. J. Geophys. Res. 105, 3059–3079.

Kennett, J.P., Burns, R.E., Andrews, J.E., Churkin, M., Davies, T.A., Dumitrica, P., Edwards, A.R., Galehouse, J.S., Packham, G.H., Van der Linger, G.J., 1972. Australian–Antarctic continental drift, palaeocirculation changes and Oligocene deep-sea erosion. Nature 239, 51–55.

Kennett, J.P., 1982. Marine Geology. Prentice-Hall, Englewood Cliffs, NJ p. 813.

Lagabrielle, Y., Goddéris, Y., Donnadieu, Y., Malavieille, J., Suarez, M., 2009. The tectonic history of Drake Passage and its possible impacts on global climate. Earth Planet. Sci. Lett. 279 (3), 197–211.

Lee, T.Q., Kissel, C., Barrier, E., Laj, C., Chi, W.R., 1991. Paleomagnetic evidence for a diachronic clockwise rotation of the Coastal Range, eastern Taiwan. Earth Planet. Sci. Lett. 104 (2), 245–257.

Li, Q., Wang, P., Zhao, Q., Shao, L., Zhong, G., Tian, J., Cheng, X., Jian, Z., Su, X., 2006. A 33 Ma lithostratigraphic record and paleoceanographic evolution of the South China Sea. Mar. Geol. 230, 217–235. http://dx.doi.org/10.1016/j.margeo.2006.05.006.

Li, Q., Zhao, Q., Zhong, G., Jian, Z, Tian, J., Cheng, X., Wang, P., Chen, M., 2007. Deepwater ventilation and stratification in the Neogene South China Sea. J. China Univ. Geosci. 18 (2), 95–108.

Li, Q., Wang, P., Zhao, Q., Tian, J., Cheng, X., Jian, Z., Zhong, G., Chen, M., 2008. Paleoceanography of the mid-Pleistocene South China Sea. Quat. Sci. Rev. 27 (11), 1217–1233.

Lin, A.T., Watts, A.B., Hesselbo, S.P., 2003. Cenozoic stratigraphy and subsidence history of the South China Sea margin in the Taiwan region. Basin Res. 15, 453–478. http://dx.doi.org/10.1046/j.1365-2117.2003.00215.x.

Lin, W.H., Lin, C.W., Liu, Y.C., Chen, P.T., 2008. Explanatory Text of the Geologic Map of Taiwan, Scale 1:50 000. Taitung and Jhihben Sheet. Central Geology Survey, MOEA.
Linthout, K., Helmers, H., Sopaheluwakan, J., 1997. Late Miocene obduction and microplate migration around the southern Banda Sea and the closure of the Indonesian Seaway. Tectonophysics 281 (1), 17–30.
Lo, C.H., Onstott, T.C., Chen, C.H., Lee, T., 1994. An assessment of $^{40}Ar/^{39}Ar$ dating for the whole-rock volcanic samples from the Luzon Arc near Taiwan. Chem. Geol. 114, 157–178.
Martini, E., 1971. Standard Tertiary and Quaternary calcareous nannoplankton zonation. In: Farinacci, A. (Ed.), Proceedings of the 2nd International Conference on Planktonic Microfossils, vol. 2. Ed. Tecnosci., Roma, pp. 739–785.
Miller, K.G., Fairbanks, R.G., 1985. Oligocene to Miocene carbon isotope cycles and abyssal circulation changes. In: Sundquist, E.T., Broecker W.S. (Eds.), The Carbon Cycle and Atmospheric CO_2: Natural Variations Archean to Present. AGU Geophysical Monograph Series 32, Washington DC, pp. 469–486.
Poore, H.R., Samworth, R., White, N.J., Jones, S.M., McCave, I.N., 2006. Neogene overflow of Northern Component Water at the Greenland–Scotland Ridge. Geochem. Geophys. Geosyst. 7, Q06010. http://dx.doi.org/10.1029/2005GC001085.
Qu, T., Girton, J.B., Whitehead, J.A., 2006. Deepwater overflow through Luzon Strait. J. Geophys. Res. 111, C01002. http://dx.doi.org/10.1029/2005JC003139.
Reed, D.L., Lundberg, N., Liu, C.S., Luo, B.Y., 1992. Structural relations along the margins of the offshore Taiwan accretionary wedge: implications for accretion and crustal kinematics. Acta Geol. Taiwan 30, 105–122.
Ryan, W.B.F., Carbotte, S.M., Coplan, J.O., O'Hara, S., Melkonian, A., Arko, R., Weissel, R.A., Ferrini, V., Goodwillie, A., Nitsche, F., Bonczkowski, J., Zemsky, R., 2009. Global multi-resolution topography synthesis. Geochem. Geophys. Geosyst. 10, Q03014. http://dx.doi.org/10.1029/2008GC002332.
Schnűrle, P., Liu, C.S., Lallemand, S., Reed, D., 1998. Structural controls of the Taitung Canyon in the Huatung Basin east of Taiwan. Terr. Atmos. Ocean. Sci. 9, 453–472.
Shackleton, N.J., 1977. Tropical rainforest history and the equatorial Pacific carbonate dissolution cycles. In: Andersen, N.R., Malahoff, A. (Eds.), The Fate of Fossil Fuel CO_2 in the Oceans. Plenum, New York, pp. 401–428.
Sheu, D.D., Lee, W.Y., Wang, C.H., Wei, C.L., Chen, C.T.A., Cherng, C., Huang, M.H., 1996. Depth distribution of $\delta^{13}C$ of dissolved ΣCO_2 in seawater off eastern Taiwan: effects of the Kuroshio current and its associated upwelling phenomenon. Cont. Shelf Res. 16 (12), 1609–1619.
Suppe, J., 1981. Mechanics of mountain building and metamorphism in Taiwan. Mem. Geol. Soc. China 4, 67–89.
Suppe, J., 1984. Kinematics of arc–continent collision, flipping of subduction, and back-arc spreading near Taiwan. Mem. Geol. Soc. China 6, 21–33.
Taylor, B., Hayes, D.E., 1983. Origin and history of the South China Sea basin. In: Hayes, D.E. (Ed.), The Tectonic and Geologic Evolution of Southeast Asian Seas and Islands: Part 2. AGU Geophysical Monograph Series 27, Washington DC, pp. 23–56.
Teng, L.S., 1990. Geotectonic evolution of late Cenozoic arc–continent collision in Taiwan. Tectonophysics 183, 57–76.
Tian, J., Yang, Q., Liang, X., Xie, L., Hu, D., Wang, F., Qu, T., 2006. Observation of Luzon Strait transport. Geophys. Res. Lett. 33, L1960. http://dx.doi.org/10.1029/2006GL026272.
Tian, J., Zhao, Q., Wang, P., Li, Q., Cheng, X., 2008. Astronomically modulated Neogene sediment records from the South China Sea. Paleoceanography 23, PA3210. http://dx.doi.org/10.1029/2007PA001552.
Tian, J.W., Qu, T.D., 2012. Advances in research on the deep South China Sea circulation. Chin. Sci. Bull. 57, 3115–3120. http://dx.doi.org/10.1007/s11434-012-5269-x.
Tsai, Y.B., 1986. Seismotectonics of Taiwan. Tectonophysics 125 (1), 17–37.
Wade, B.S., Pearson, P.N., Berggren, W.A., Pälike, H., 2011. Review and revision of Cenozoic tropical planktonic foraminiferal biostratigraphy and calibration to the geomagnetic polarity and astronomical time scale. Earth-Sci. Rev 104, 111–142. http://dx.doi.org/10.1016/j.earscirev.2010.09.003.
Wang, P., Zhao, Q., Jian, Z., Cheng, X., Huang, W., Tian, J., Wang, J., Li, Q., Li, B., Su, X., 2003. Thirty million year deep sea records in the South China Sea. Chin. Sci. Bull. 48 (23), 2524–2535. http://dx.doi.org/10.1360/03wd0154.
Wang, P.X., 2012. Tracing the life history of a marginal sea—on the "South China Sea Deep" Research Program. Chin. Sci. Bull. 57, 3093–3114. http://dx.doi.org/10.1007/s11434-012-5087-1.
Wei, G.J., Huang, C.Y., Wang, C.C., Lee, M.Y., Wei, K.Y., 2006. High-resolution benthic foraminifer $\delta^{13}C$ records in the South China Sea during the last 150 ka. Mar. Geol. 23, 227–235. http://dx.doi.org/10.1016/j.margeo.2006.08.005.
Wyrtki, K., 1961. Physical Oceanography of the Southeast Asian Waters. Scientific Results of Marine Investigations of the South China Sea and the Gulf of Thailand 1959–1961. Naga Rep. 2. Scripps Institution of Oceanography, La Jolla, California 195 pp.
Yang, K.M., Wang, Y., Tsai, Y.B., Hsu, V., 1983. Paleomagnetic studies of the Coastal Range, Lutao and Lanhsu in eastern Taiwan and their tectonic implications. Bull. Inst. Earth Sci. Acad. Sin. 3, 173–189.
Yang, K.M., Wu, J.C., Cheng, E.W., Chen, Y.R., Huang, W.C., Tsai, C.C., Wang, J.B., Ting, H.H., 2014. Development of tectonostratigraphy in distal part of foreland basin in southwestern Taiwan. J. Asian Earth Sci. 88, 98–115. http://dx.doi.org/10.1016/j.jseaes.2014.03.005.
Yang, T.F., Tien, J.L., Chen, C.H., Lee, T., Punongbayan, R.S., 1995. Fission-track dating of volcanics in the northern part of the Taiwan–Luzon arc: eruption ages and evidence for crustal contamination. J. Sotheast Asian Earth Sci. 11 (2), 81–93.
Yang, T.Y., Liu, T.K., Chen, C.H., 1988. Thermal event records of the Chimei igneous complex: constraint on the ages of magma activities and structural implication based on fission track dating. Acta Geol. Taiwan 26, 237–246.
Yu, S.B., Chen, H.Y., Kuo, L.C., 1997. Velocity field of GPS stations in the Taiwan area. Tectonophysics 274, 41–59.
Yumul Jr., G.P., Dimalanta, C.B., Marquez, E.J., Queaño, K.L., 2009. Onland signatures of the Palawan microcontinental block and Philippine mobile belt collision and crustal growth process: a review. J. Asian Earth Sci. 34 (5), 610–623.
Zachos, J., Pagani, M., Sloan, L., Thomas, E., Billups, K., 2001. Trends, rhythms, and aberrations in global climate 65 Ma to present. Science 292, 686–693. http://dx.doi.org/10.1126/science.1059412.
Zhao, Q., Wang, P., Cheng, X., Wang, J., Huang, B., Xu, J., Zhou, Z., Jian, Z., 2001. A record of Miocene carbon excursions in the South China Sea. Sci. China Ser. D—Earth Sci. 44 (10), 943–951.
Zhao, Q., Li, Q., Jian, Z., 2009. Deep waters and oceanic connection. In: Wang, P., Li, Q. (Eds.), The South China Sea: Paleoceanography and Sedimentology. Springer, Berlin, pp. 395–437.
Zhao, W., Zhou, C., Tian, J., Yang, Q., Wang, B., Xie, L., Qu, T., 2014. Deep water circulation in the Luzon Strait. J. Geophys. Res. Oceans 119, 790–804. http://dx.doi.org/10.1002/2013JC009587.